(12)

B.S.

LEVEL II

ENSCO, INC.

APPROVED FOR PUBLIC RELEASE, DISTRIBUTION UNLIMITED

SAR(01)-TR-79-03
16 October 1979

APPLICATION OF THE PHASE-DIFFERENCE POLARIZATION FILTER TO SHORT-PERIOD REGIONAL DATA

TECHNICAL REPORT NO. 3

PREPARED BY
ALAN C. STRAUSS

PREPARED FOR
AIR FORCE TECHNICAL APPLICATIONS CENTER
ALEXANDRIA, VIRGINIA 22314

ENSCO, INC.
SEISMIC APPLIED RESEARCH DIVISION
813 NORTH ROYAL STREET
ALEXANDRIA, VIRGINIA 22314

UNCLASSIFIED

SECURITY CLASSIFICATION OF THIS PAGE (When Data Entered)

REPORT DOCUMENTATION PAGE

READ INSTRUCTIONS BEFORE COMPLETING FORM

1. REPORT NUMBER (6)

2. GOVT ACCESSION NO.

3. RECIPIENT'S CATALOG NUMBER

(11 Dec 78 - 31 Mar 80)

4. TITLE (and Subtitle)

APPLICATION OF THE PHASE-DIFFERENCE POLARIZATION FILTER TO SHORT-PERIOD REGIONAL DATA

5. TYPE OF REPORT & PERIOD COVERED

(9) Technical rept.

6. PERFORMING ORG. REPORT NUMBER

(14) SAR(01)-TR-79-03, TR-3

7. AUTHOR(s)

(10) Alan C. Strauss

8. CONTRACT OR GRANT NUMBER(s)

(15) F08606-79-C-0014, ARPA Order-2551

9. PERFORMING ORGANIZATION NAME AND ADDRESS

ENSCO, INC.
SAR Division
Alexandria, Virginia 22314

10. PROGRAM ELEMENT, PROJECT, TASK AREA & WORK UNIT NUMBERS

VELA T/9705/B/PMP

11. CONTROLLING OFFICE NAME AND ADDRESS

Advanced Research Projects Agency
Nuclear Monitoring Research Office
Arlington, Virginia 22209

(11) 12. REPORT DATE

16 October 1979

13. NUMBER OF PAGES

75

14. MONITORING AGENCY NAME & ADDRESS(if different from Controlling Office)

Air Force Technical Applications Center
VELA Seismological Center
Alexandria, Virginia 22314

15. SECURITY CLASS. (of this report)

UNCLASSIFIED

15a. DECLASSIFICATION/DOWNGRADING SCHEDULE

16. DISTRIBUTION STATEMENT (of this Report)

(12) 78

APPROVED FOR PUBLIC RELEASE, DISTRIBUTION UNLIMITED

17. DISTRIBUTION STATEMENT (of the abstract entered in Block 20, if different from Report)

18. SUPPLEMENTARY NOTES

ARPA Order No. 2551

19. KEY WORDS (Continue on reverse side if necessary and identify by block number)

Seismology	Signal-To-Noise Ratio Gains
Regional Phases	Detection Capability
Signal Extraction	Polarization Filtering
Mixed Signals	Filtering

20. ABSTRACT (Continue on reverse side if necessary and identify by block number)

The purpose of this work is to optimize the phase-difference polarization filter for use in extracting short-period regional data from seismic noise and signal coda. The phases to be extracted are the bodywaves Pn, Pg, Sn, and Sg, and the surface waves Lg and Rg. The data available for this work were from events with epicenters in northeastern China, and in Honshu and Hokkaido, Japan. The data used were

DD FORM 1 JAN 73 1473 EDITION OF 1 NOV 65 IS OBSOLETE

UNCLASSIFIED

SECURITY CLASSIFICATION OF THIS PAGE (When Data Entered)

411669

AM

20. (continued)

recorded at the three-component short-period site of the Korean Seismic Research Station (KSRS). The polarization filter yields signal-to-noise ratio gains of approximately 10 dB for regional compressional and shear waves (Pn, Pg, Sn, and Sg) and of approximately 8 dB for regional surface waves (Lg and Rg). Direct estimates of the detection capability for regional P and S ($\Delta=10^{o}$ to 13^{o}) made before and after polarization filtering show that the polarization filter yields detection improvements of approximately 0.6 m_b units for these phases. Finally, the polarization filter can be used to separate mixed signals, to identify phases, and to extract regional phases from seismic noise.

This research was supported by the Advanced Research Projects Agency of the Department of Defense and was monitored by AFTAC/VSC, Patrick Air Force Base, FL 32925, under Contract Number F08606-79-C-0014.

AFTAC Project Number:	VELA T/9705/B/PMP
Project Title:	VELA Network and Automatic Processing Research
ARPA Order Number:	2551
Name of Contractor:	ENSCO, Incorporated
Contract Number:	F08606-79-C-0014
Effective Date of Contract:	11 December 1978
Contract Expiration Date:	31 March 1980
Project Manager:	Theodore J. Cohen (703) 548-8666

SUMMARY

The purpose of this work is to optimize the phase-difference polarization filter for use in extracting short-period regional data from seismic noise and signal coda. The phases to be extracted are the bodywaves Pn, Pg, Sn, and Sg, and the surface waves Lg and Rg. The data available for this work were from events with epicenters in northeastern China, and in Honshu and Hokkaido, Japan. The data used were recorded at the three-component short-period site of the Korean Seismic Research Station (KSRS). The polarization filter yields signal-to-noise ratio gains of approximately 10 dB for regional compressional and shear waves (Pn, Pg, Sn, and Sg) and of approximately 8 dB for regional surface waves (Lg and Rg). Direct estimates of the detection capability for regional P and S ($\Delta=10^{\circ}$ to 13°) made before and after polarization filtering show that the polarization filter yields detection improvements of approximately 0.6 m_b units for these phases. Finally, the polarization filter can be used to separate mixed signals, to identify phases, and to extract regional phases from seismic noise.

TABLE OF CONTENTS

SECTION	TITLE	PAGE
	SUMMARY	iii
I.	INTRODUCTION	I-1
	A. SUMMARY OF PREVIOUS WORK	I-1
	B. GOALS	I-3
II.	METHODOLOGY	II-1
	A. DESCRIPTION OF THE METHOD	II-1
	B. POLARIZATION FILTER OPTIMIZATION	II-9
III.	THE EFFECTS OF POLARIZATION FILTERING ON SIGNAL-TO-NOISE RATIO AND DETECTION CAPABILITY	III-1
IV.	EXAMPLES OF POLARIZATION FILTER USAGE	IV-1
V.	CONCLUSIONS AND RECOMMENDATIONS	V-1
	A. CONCLUSIONS	V-1
	B. RECOMMENDATIONS FOR FUTURE USE	V-2
VI.	REFERENCES	VI-1
Appendix A	THE POLARIZATION FILTER PROGRAM	A-1

LIST OF FIGURES

FIGURE	TITLE	PAGE
II-1	SEPARATION OF REGIONAL SEISMIC PHASES BY PHASE ANGLE DIFFERENCE	II-2
II-2	POLARIZATION FILTER TRAPEZOIDAL PASS WINDOW	II-4
II-3	PICTORIAL REPRESENTATION OF POLARIZATION FILTER	II-5
II-4	LOVE WAVE ARRIVAL AZIMUTH FOR AN ARBITRARY FREQUENCY COMPONENT	II-8
II-5	COMPARISON OF THREE BANDPASS FILTERS CASCADED WITH THE PHASE-DIFFERENCE POLARIZATION FILTER (VERTICAL COMPONENT)	II-12
II-6	EFFECTS OF CHANGING NUMBER OF POINTS PER PROCESSING SEGMENT ON POLARIZATION FILTER RESULTS	II-17
III-1	EXAMPLES OF COMPOSITE DATA BEFORE AND AFTER POLARIZATION FILTERING	III-3
III-2	POLARIZATION FILTER GAIN AS A FUNCTION OF TRUE INPUT SIGNAL-TO-NOISE RATIO	III-4
III-3	COMPRESSIONAL WAVEFORM POLARIZATION FILTER GAIN CURVES FOR Pg, Pn, AND REGIONAL P	III-6
III-4	SHEAR WAVEFORM POLARIZATION FILTER GAIN CURVES FOR Sn AND REGIONAL S	III-8
III-5	REPRESENTATIVE SAMPLE Lg, Sg, AND Rg WAVEFORMS FOR $\Delta<10^{\circ}$	III-10
III-6	P-WAVE DETECTION STATISTICS	III-15
III-7	S-WAVE DETECTION STATISTICS	III-16
IV-1	EXTRACTION OF Pn AND Pg PHASES	IV-3
IV-2	EXTRACTION OF Sn FROM P-CODA AND SEISMIC NOISE	IV-4

LIST OF FIGURES
(continued)

FIGURE	TITLE	PAGE
IV-3	EXTRACTION OF Sg, Lg, AND Rg FROM SHEAR CODA AND SEISMIC NOISE	IV-6
IV-4	EXTRACTION OF Pg FROM Pn-CODA	IV-7
IV-5	P CONVERSION TO OTHER PROPAGATION MODES	IV-8
IV-6	P GATE OF REPORTED HONSHU, JAPAN EVENT	IV-10
IV-7	S GATE OF REPORTED HONSHU, JAPAN EVENT	IV-11
IV-8	DATA FOR MIXED SIGNAL SEPARATION	IV-13
IV-9	P GATE OF EVENT OF FIGURE IV-8	IV-14
IV-10	Sn-Rg GATE OF EVENT OF FIGURE IV-8	IV-15
IV-11	POST-Lg, Rg GATE OF EVENT OF FIGURE IV-8	IV-16
A-1	GENERALIZED FLOW OF PHASE-DIFFERENCE POLARIZATION FILTER	A-2
A-2	DETAILED FLOW OF POLARIZATION FILTER ALGORITHM	A-4
A-3	POLARIZATION FILTER TRAPEZOIDAL PASS WINDOW	A-6

LIST OF TABLES

TABLE	TITLE	PAGE
II-1	TEST OF POLARIZATION FILTER WITH AND WITHOUT PRECEDING BANDPASS FILTER	II-10
II-2	SIGNAL-TO-NOISE RATIO GAINS PRODUCED BY VARIOUS COMBINATIONS OF THE POLARIZATION FILTER PARAMETERS	II-16
III-1	EFFECTS OF POLARIZATION FILTER ON THE SIGNAL-TO-NOISE RATIOS OF REGIONAL PHASES	III-12

SECTION I
INTRODUCTION

A. SUMMARY OF PREVIOUS WORK

This research effort is intended to refine and test a technique to extract and identify the short-period regional phases Pn, Pg, Sn, Sg, Lg, and Rg. The technique, called phase-difference polarization filtering, was originally developed for long-period teleseismic data (Strauss, 1978). However, with the move toward utilization of three-component single-site stations, and with the increased interest in regional seismic data, it becomes desirable to apply the technique to short-period regional phases.

An earlier form of polarization filtering, used to extract compressional and shear waves, operated on the expected angles of incidence of these bodywaves (Lane, 1977; Strauss, 1978). When tested on long-period teleseismic data, however, the performance of this filter proved to be regionally dependent; it showed little change in detection capability for Kurile-Kamchatka events as recorded at Guam and 0.3-0.4 m_b units improvement for the same events as recorded at Mashhad, Iran.

Practical considerations dictate that the first step in designing regional short-period polarization filters should be to use only universally applicable criteria. Such an approach is described below.

Specifically, the phase-difference polarization filter developed for regional phases is a logical extension of the three-component adaptive processor designed by Lane (1973, 1976). This processor searches for long-period waveforms which display a 90^{o} phase difference between the radial and vertical components of motion, as is exhibited by Rayleigh waves (retrograde elliptical waveforms). To extract compressional waveforms, the sought-for phase difference is set to 0^{o}, while to extract shear waveforms, the sought-for phase difference is set to 180^{o}. To extract prograde elliptical waveforms, the sought-for phase difference is set to 270^{o}. A separate algorithm, which passes only that energy which is within a specified range about the predicted arrival azimuth, is used to extract Lg data recorded on the transverse component. A detailed description of this filter technique is presented in Section II.

Previous applications of the phase-difference polarization filter to long-period teleseismic data gave a 0.5 m_b unit improvement (approximate) in detection capability for P, S, and LR waveforms (Strauss, 1978). Preliminary testing of this filter on short-period regional data indicated that the same improvement in detection capability might be expected. In addition, preliminary tests indicated that the polarization filter may be useful in waveform identification (e.g., a waveform passed by the P model of the filter can be more confidently identified as a P wave).

B. GOALS

This report presents the results of research on the application of the phase-difference polarization filter to regional short-period data. The specific goals of this study were:

- To design three-component adaptive filters which extract short-period regional phase signals;
- To estimate the effects of such filters on the detection capability of the phases Pn, Pg, Sn, Sg, Lg, and Rg;
- To test the filters on seismic events with epicentral distances between 0° and 20° from the receiver site;
- To outline future, feasible extensions of polarization filter use to the problem of identifying significantly refracted or wave-guided phases which are observed at regional distances (this pertains to source discrimination by correlation with source-region-to-station synthetics).

To accomplish the first goal, the existing long-period teleseismic polarization filter was adapted to process short-period regional data. The intent is to find those values of the polarization filter program parameters which produce maximum signal-to-noise ratio (SNR) gains consistent with relatively low variance in these gains from event to event. This work is described in Section II.

Work performed toward achieving the second goal was directed toward optimizing the performance of polarization

filters by determining the improvement in signal-to-noise ratio produced by application of the polarization filter. This was accomplished by applying the filter to a suite of synthetic seismograms. In this approach, a test signal is scaled and added to noise in order to produce a synthetic signal of known peak signal-to-RMS-noise ratio (SNR). Varying the scaling allows one to create a suite of signals which differ only in SNR. Processing such a suite of data with the polarization filter then permits accurate gauging of SNR improvement which can be achieved through application of the filter. More significantly, detection capability improvement is accurately gauged by noting the input SNR of the smallest detectable signal before and after filter application.

The test data available for this task consisted of three-component short-period data recorded at the Korean Seismic Research Station (KSRS). The majority of the regional events for which data were available had epicenters near Honshu, Japan ($\Delta=10^{o}$ to 13^{o}). A source region in northeastern China ($\Delta\sim8^{o}$) provided data for approximately 50 events. Relatively little data were available for epicentral distances less than 7^{o}. Thus, the data available were sufficient to allow an estimation of detection capability improvement produced by application of the polarization filter for P and S phases observed at regional distances. These direct estimates of detection capability improvement are used to verify the estimates derived from the improvements determined using synthetic seismograms. Work performed on the second goal is described in Section III.

The purpose of the third goal is to illustrate the capability of the polarization filter to extract and identify phases and to separate mixed signals. This work is described in Section IV.

Finally, the conclusions reached from this work are presented in Section V. This section also presents recommendations for future work involving the phase-difference polarization filter and other feasible extensions of the polarization filter concept.

It should be noted that all computer processing performed during the course of this task was carried out in a batch processing environment. Where pertinent, the differences between this type of processing environment and an interactive environment will be noted.

SECTION II
METHODOLOGY

A. DESCRIPTION OF THE METHOD

The polarization filter described in this report depends on the phase difference between the radial and vertical signatures for extracting compressional, shear, retrograde elliptical, and prograde elliptical short-period regional signals. A separate algorithm, described below, is used to extract Lg. Figure II-1 summarizes the four models available in the polarization filter.

Let the radial and vertical Fourier transform for any given time segment be represented by:

$$R(\omega) = A_R(\omega)\, e^{-j\omega_o t + \phi_R(\omega)}$$

$$V(\omega) = A_V(\omega)\, e^{-j\omega_o t + \phi_V(\omega)}$$

where ω_o is an arbitrary reference frequency and $\phi_R(\omega)$ and $\phi_V(\omega)$ are the radial and vertical instantaneous phases with respect to ω_o. Thus, the radial and vertical components at any given frequency differ in phase by $[\phi_R(\omega) - \phi_V(\omega)]$. To extract the short-period regional waveforms, the test statistic

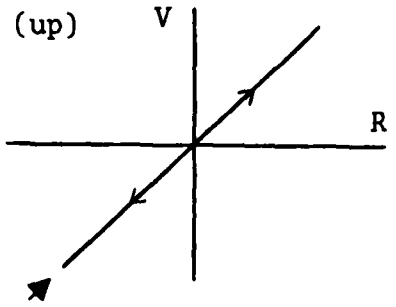

Compressional Model

0^{o} phase angle difference separates Pn and Pg phases as compressional waves

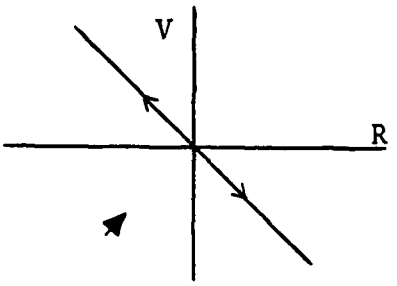

Shear Model

180^{o} phase angle difference separates Sn and Sg phases as shear waves

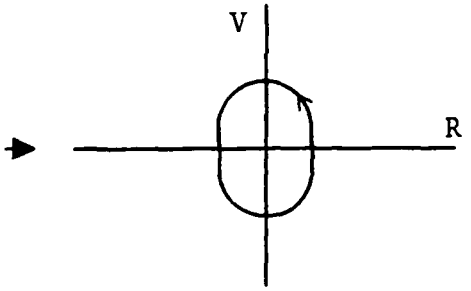

Retrograde Elliptical Model

90^{o} phase angle difference separates Rayleigh waves by elliptical retrograde particle motion

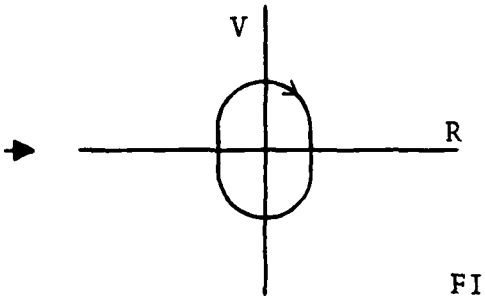

Prograde Elliptical Model

270^{o} phase angle difference separates leaky modes by elliptical prograde particle motion

FIGURE II-1

SEPARATION OF REGIONAL SEISMIC PHASES BY PHASE ANGLE DIFFERENCE

$$\phi_o(\omega) = |\phi_R(\omega) - \phi_V(\omega)| \quad \text{for compressional waves}$$

$$\phi_o(\omega) = |\phi_R(\omega) - \phi_V(\omega) - \pi/2| \quad \text{for retrograde elliptical waves}$$

$$\phi_o(\omega) = |\phi_R(\omega) - \phi_V(\omega) - \pi| \quad \text{for shear waves, or}$$

$$\phi_o(\omega) = |\phi_R(\omega) - \phi_V(\omega) - 3\pi/2| \quad \text{for prograde elliptical waves}$$

is computed. If $\phi_o(\omega)$ is less than some pre-set value α_o, a filter weight of '1' is assigned to the data. If $\phi_o(\omega)$ is greater than α_o but less than some value α_1, a filter weight between zero and '1' is assigned; the value of the filter weight depends on the separation between $\phi_o(\omega)$ and α_o. If $\phi_o(\omega)$ is greater than α_1, a filter weight of zero is assigned. Thus, the pass window is trapezoidal in shape (see Figure II-2). This procedure allows the acceptance of signals whose phase difference does not exactly meet the appropriate model because of noise-induced distortions. A pictorial overview is presented in Figure II-3; a detailed description of the polarization filter program is presented in Appendix A.

Note that the amount of noise suppression to be realized can be predicted for this filter. For noise with random radial-vertical phase differences, $\phi_o(\omega)$ will range between 0^o and 180^o. Values of 15^o for α_o and α_1 imply that one-eighth of the noise will be passed by the polarization filter ($(\alpha_o + \alpha_1/2)/180$, since the filter weights between α_o and α_1 decrease linearly toward zero). Rejection of seven-eights of the noise corresponds to a 9 dB noise suppression.

The concept of polarization filtering may further be described by considering signals and noise as a superposition

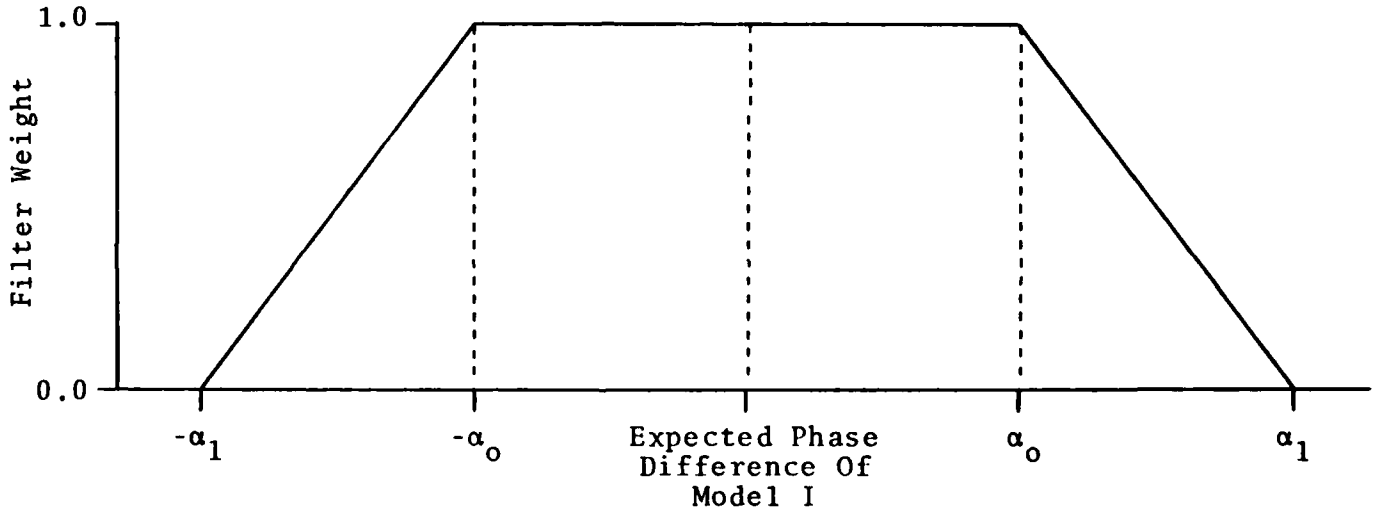

FIGURE II-2

POLARIZATION FILTER TRAPEZOIDAL PASS WINDOW
(α_o, α_1 are preset filter parameters)

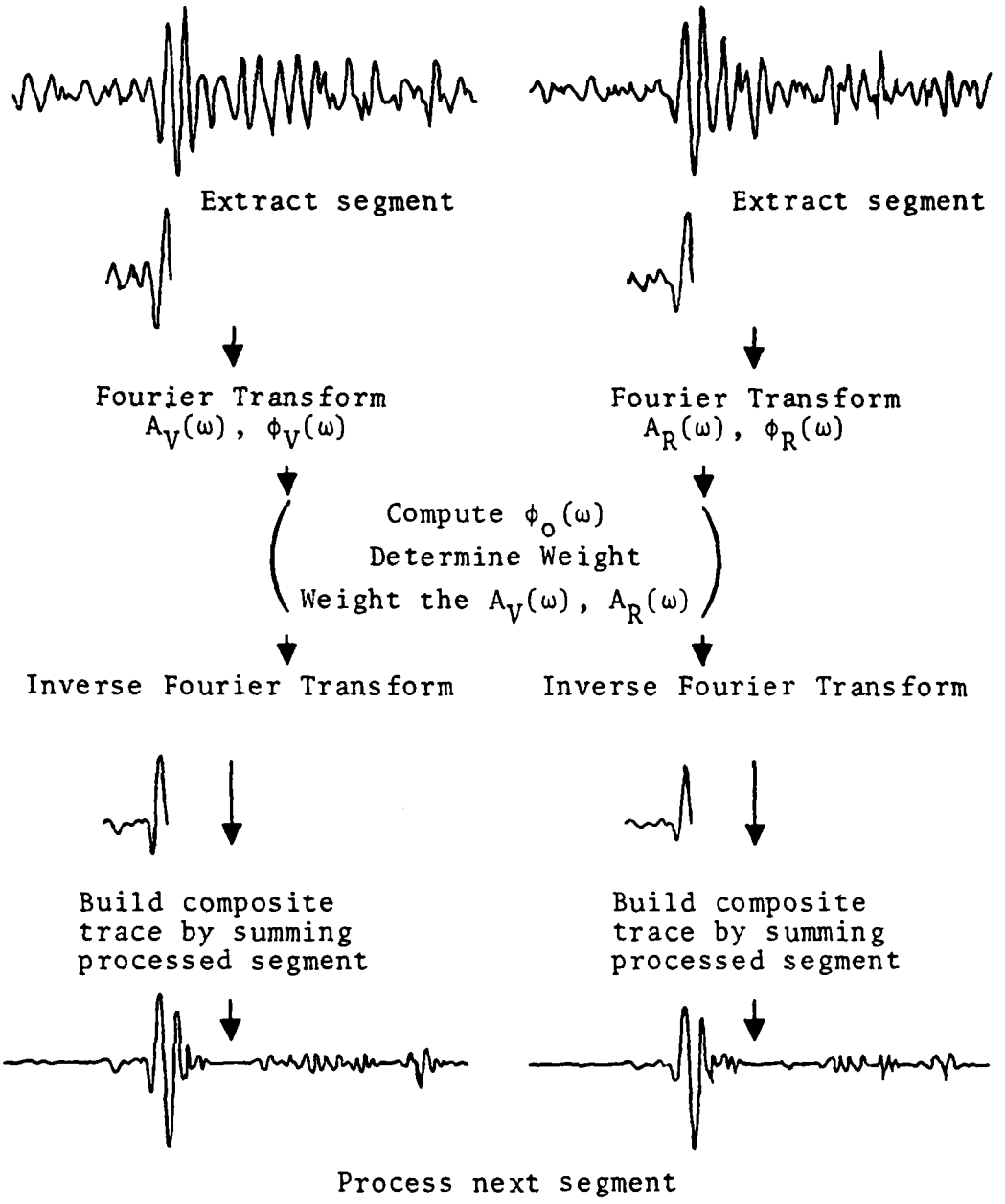

FIGURE II-3
PICTORIAL REPRESENTATION OF POLARIZATION FILTER

of modulated amplitude and phase components. The radial and vertical time traces are given as follows:

$$r(t) = \sum_i A_R(t,\omega_i)\, e^{-j\,\omega_i t+\phi_R(t,\omega_i)}$$

$$v(t) = \sum_i A_V(t,\omega_i)\, e^{-j\,\omega_i t+\phi_V(t,\omega_i)} \quad .$$

If at any time a regional phase occurs where the radial and vertical component exceeds noise on one or more of the spectral components, then the desired phase relationship is satisfied and the signal component is passed without distortion. The threshold for satisfying the phase relationship must be set wide enough to pass imperfect signals and yet narrow enough to reject chance correlations of random phase noise. For example, given a phase relationship for P waves of zero, experience may indicate that at least a $\pm 15^{o}$ passband is needed to pass signals without distortion ($\alpha_o = \alpha_1 = 15^{o}$, in this case). Further, assume that noise is equally likely to exhibit any phase angle between 0^{o} and 360^{o}. Then the probability of noise passing the signal criteria is 1/12. Thus, only $1/12^{th}$ of the spectral noise components are weighted by one; the other $11/12^{ths}$ are weighted zero. By application of Parseval's theorem (Brand, 1955) the variance of noise in the time domain is reduced to $1/12^{th}$ of what it was before applying the phase angle criteria of polarization filters. Therefore, the theoretical gain expected by polarization filters in this case is $10 \log_{10}(1/12) = 10.8$ dB. An interesting result of this very simple noise model is that this gain of 0.5 to 0.6 m_b units of improvement would be expected for any propagation mode to which this criteria is applied; the reason for this is that the random phase of the noise is independent of the propagation mode to be extracted. Experience (Strauss, 1977)

with long-period surface wave extraction as well as short-period regional phase extraction indicates this to be the case. Some variation from this expected gain might be encountered in cases where the radial and vertical components differ greatly. For example, if $A_V >> A_R$ as for teleseismic P waves, higher signal-to-noise ratios would be required for both components to dominate the noise. In such a case, the expected gain would be considerably less than predicted. For long-period surface waves and the regional phases extracted by this criteria, $A_V \approx A_R$.

To extract Lg, the assumption is made that Lg is the short-period analog of the long-period Love wave. As shown in Figure II-4, the apparent arrival azimuth of the Love (Lg) wave can be expected to show small deviations (β) from the arrival azimuth predicted from the event epicenter and receiver location. Noise, however, will produce values of β varying randomly from 0^o to 360^o. The algorithm used to extract Lg waves, therefore, computes this angle β on a frequency-by-frequency basis using

$$\beta = \tan^{-1} \frac{R_r}{T_r} \quad ,$$

where R_r is the real part of the Fourier transform of the radial component while T_r is the real part of the transform of the transverse component.

The computed value of β is used to assign a filter weight to the Fourier amplitude at the frequency from which it was computed, where the filter weight is determined in the same fashion as previously described. This algorithm is discussed in detail by Strauss (1976).

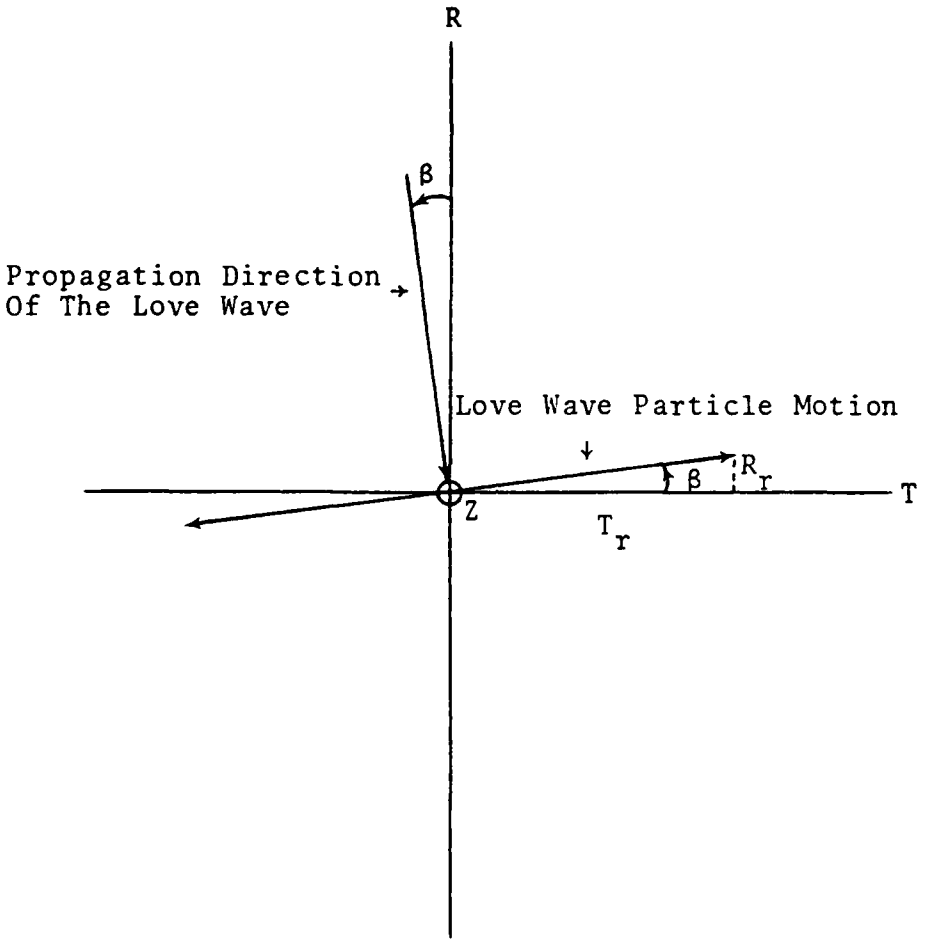

FIGURE II-4

LOVE WAVE ARRIVAL AZIMUTH FOR AN
ARBITRARY FREQUENCY COMPONENT

B. POLARIZATION FILTER OPTIMIZATION

It now remains to optimize the performance of the polarization filter (in terms of producing the greatest SNR). Optimization of the filter will free the analyst from the necessity to repeatedly process each event in order to obtain the 'best' result. In optimizing the use of the polarization filter, minimal prior knowledge of the signal to be processed is assumed (all that must be known about the data is the source location since the filter does require data rotated to a vertical, transverse, radial configuration).

It has been demonstrated (Lane, 1977) for long-period signal extraction applications that a bandpass prefilter produces greater SNR improvements than does application of a polarization-type filter alone. Whether this holds true in the case of short-period regional data must be examined, and, if it does, the question of what bandpass filter serves as the best prefilter must be answered.

Table II-1 shows the results of processing a suite of regional P waves and a suite of regional S waves ($\Delta \sim 10^{o}$) using the polarization filter. Each data set was processed once with the polarization filter applied to the raw data, and once with the polarization filter applied to bandpass-filtered data. As is seen, the bandpass/polarization filter cascaded combination produces higher SNR gains with lower variance in the gains than does the polarization filter alone. Thus, it appears desirable to preprocess data using a bandpass filter prior to applying the polarization filter.

The bandpass filter used in the above test was a broadband type having a passband of 0.5-5.0 Hz and a 10-point

TABLE II-1

TEST OF POLARIZATION FILTER WITH AND WITHOUT PRECEDING BANDPASS FILTER

		Data Processed Without Bandpass Filter			Data Processed First With 0.5-5.0 Hz Bandpass Filter		
		Noise Suppression	Signal Suppression	Net SNR Gain	Noise Suppression	Signal Suppression	Net SNR Gain
P	Mean (dB)	12.7	5.0	7.7	12.0	2.7	9.3
	Standard Deviation (dB)	3.6	2.7	4.5	3.9	1.5	4.3
S	Mean (dB)	18.1	9.0	9.1	17.8	7.1	10.7
	Standard Deviation (dB)	4.3	5.3	7.1	3.6	4.1	5.1

cosine-squared taper (data sampled at 10 samples per second). It is always possible to achieve higher SNR gains by tailoring the passband to the particular waveform to be extracted. For example, if it is known that Sn from a particular source region is dominated by 2 Hz energy at a given receiver, a narrowband filter centered on this frequency will produce higher SNR gains than will a 0.5-5.0 Hz bandpass filter. There is, however, a danger in tailoring the filter to the expected dominant frequency of the waveform since this requires prior knowledge of the spectrum of each phase from each region at each receiver. To see this, consider Figure II-5, which shows the shear wave (Sn-Sg) gate of an event from northeastern China which has been processed by the polarization filter, but which has been preceded by three different bandpass filters. Each pair of traces in this figure consists of the vertical trace after application of the bandpass filter (upper trace of each pair), and the same trace after application of the bandpass filter and the shear model of the polarization filter. The scales (S) given are the maximum amplitude of each trace in digital counts. Also shown are the SNRs for Sn and Sg, as appropriate. This figure indicates that use of an appropriately-tailored narrowband filter prior to polarization filtering yields higher SNR gains than is possible using a broadband preprocessing filter. However, note that application of the 1.25-5.0 Hz narrowband filter (center pair of traces) eliminates Sg while it enhances Sn. Further, application of the 0.5-1.25 Hz narrowband filter (bottom pair of traces) eliminates Sn while it enhances Sg. In comparison to this, the wideband filter (top pair of traces) enhances (albeit to a lesser degree) both Sn and Sg. Thus, when the polarization filter program is used in a batch processing mode, it appears preferable to use a wideband

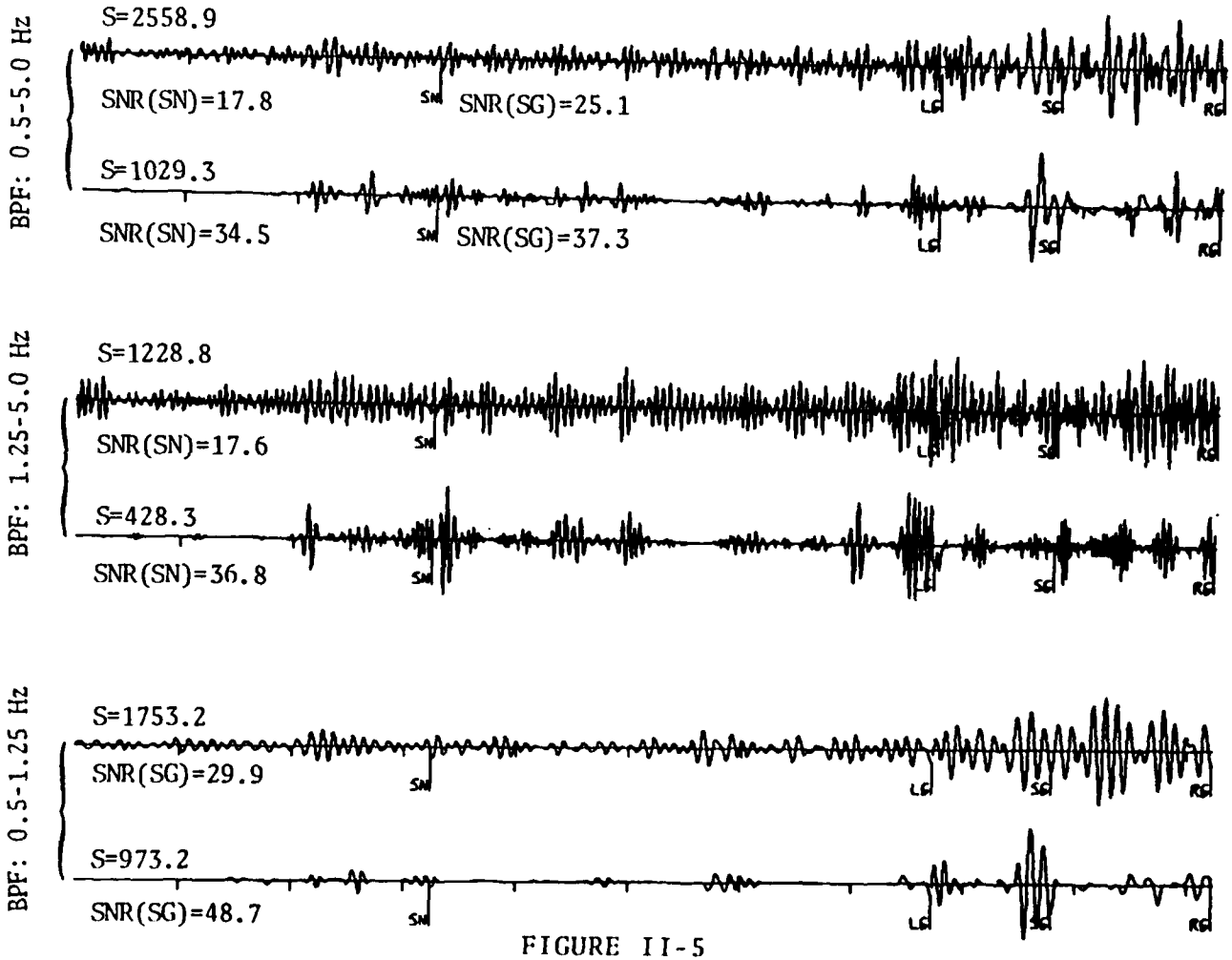

FIGURE II-5

COMPARISON OF THREE BANDPASS FILTERS CASCADED WITH THE PHASE-DIFFERENCE POLARIZATION FILTER (VERTICAL COMPONENT)

preprocessing filter. For the remainder of the work reported here (unless specifically noted), the bandpass filter used has a 0.5-5.0 Hz passband with a 10-point cosine-squared taper.

It should be noted that the use of several narrowband filters would be of great value in an interactive processing environment. Here, the analyst could select separate time gates for each phase. He could then make repeated applications of the polarization filter, using a different bandpass filter for each run in order to determine the best passband to cascade with the polarization filter for each phase. As the work progressed, the analyst would learn the best passband for each phase, and would know whether source region or source-receiver path effects impact on the choice of a passband.

The next point to be considered is the question of how the controlling parameters of the polarization filter are to be set.

The following parameters control the operation of the polarization filter algorithm: the number of points per processing segment, and the two parameters which determine the width of the trapezoidal pass window (α_o and α_1, as described earlier). Since filter weights are computed and applied on a frequency-by-frequency basis for each segment, increasing the segment length for a finite signal length has the effect of increasing the effect of noise; that is, it causes distortion of the signal phase difference. At some point, the segment length will be so long that the signal in the segment will be rejected along with the noise. On the

other hand, too short a segment length results in a less-than-optimum result. To see this, consider the case where the first few points of a signal lie near the end of a data segment. The greater part of the segment is noise, and so, these first few points of the signal will be rejected by the filter as noise. Although the next segment will contain the signal (normally a 50-percent segment overlap is used), the initial portion of the signal will be distorted due to the earlier rejection of the beginning of the signal. Thus, it is necessary to estimate the segment length at which this problem is minimized.

The effects of varying the width of the phase pass window are somewhat easier to state. The radial-vertical phase difference of any signal will, to some extent, always be distorted by the underlying noise. Widening the pass window allows more of the signal to pass; however, such widening also allows more noise to pass. In any given case, there should be a width such that the signal is passed with a minimum of accompanying noise.

The approach taken to estimate the best values for the pass windows for the various phases (in terms of maximizing the SNR) was empirical. Specifically, a suite of test data for each phase was scaled and added to noise recorded just prior to the first arrival of the signals. The resulting traces had SNRs so low that the signals could barely be seen in the noise background. The test data were then repeatedly processed using the polarization filter, with different values of the program parameters used for each run. The test values selected for the number of points per processing segment were 16, 32, and 64, while the test values initially

selected for the pass window half-width parameters (α_o=α_1) were 5^o, 10^o, 15^o, and 20^o. Note that preliminary tests revealed that the pass window half-width of 5^o produced very large variances in the mean signal-to-noise ratio values; thus, this test value for the pass window half-width was dropped from further consideration.

The results of this test are summarized in Table II-2. Note that in each test, the data were prefiltered with a 0.5-5.0 Hz bandpass filter before application of the polarization filter. The phase Lg was not separately tested since the polarization program operates on Lg and Rg in the same pass. Thus, the same program parameters are used for both phases. The phase Pg was not tested since insufficient data were available to make this test. However, in the batch processing environment used throughout this study, the parameters used to process Pn were also used to process Pg. The data of Table II-2 show that 16 points per processing segment yielded higher SNR gains than did segment lengths of 32 or 64 points.

It is instructive to examine pictorially the effect on the polarization filter output produced by varying the number of points per processing segment. With reference to Figure II-6, the top set of traces shows an Lg-Rg time gate after bandpass filtering. The three sets of traces below this first set show the polarization filter output using 16, 32, and 64 points per processing segment, respectively (the pass window half-width was set to 15^o in each case (see below)). As the processing segment length increases, the apparent length of the passed waveform increases, thereby making more difficult the picking of the phase start time (i.e., its first motion). Also, the peak amplitude of the waveform passed decreases as

TABLE II-2

SIGNAL-TO-NOISE RATIO GAINS PRODUCED BY VARIOUS COMBINATIONS OF THE POLARIZATION FILTER PARAMETERS

Parameter		P, Pn		S, Sn		Sg		Rg	
Points Per Segment	Window Width ($\alpha_o=\alpha_1$)	Mean Gain (dB)	S.D.* (dB)	Mean Gain (dB)	S.D.* (dB)	Mean Gain (dB)	S.D.* (dB)	Mean Gain (dB)	S.D.* (dB)
16	10^o	11.0	4.1	11.1	6.6	13.1	6.1	8.5	2.7
	15^o	10.4	3.4	10.5	6.0	12.8	5.4	8.1	3.0
	20^o	9.7	3.4	9.9	6.1	11.8	4.8	8.0	2.7
32	10^o	9.5	4.7	9.0	5.9	12.1	5.6	8.9	6.5
	15^o	8.8	3.6	9.1	5.9	12.1	4.2	7.4	3.3
	20^o	8.2	2.8	8.8	5.1	9.4	5.4	6.9	2.0
64	10^o	7.4	4.4	9.5	4.7	6.6	3.0	6.9	6.4
	15^o	8.2	4.2	9.0	4.2	5.7	3.0	6.7	4.9
	20^o	8.3	3.4	8.7	3.9	5.4	3.5	6.5	4.2

*Standard Deviation

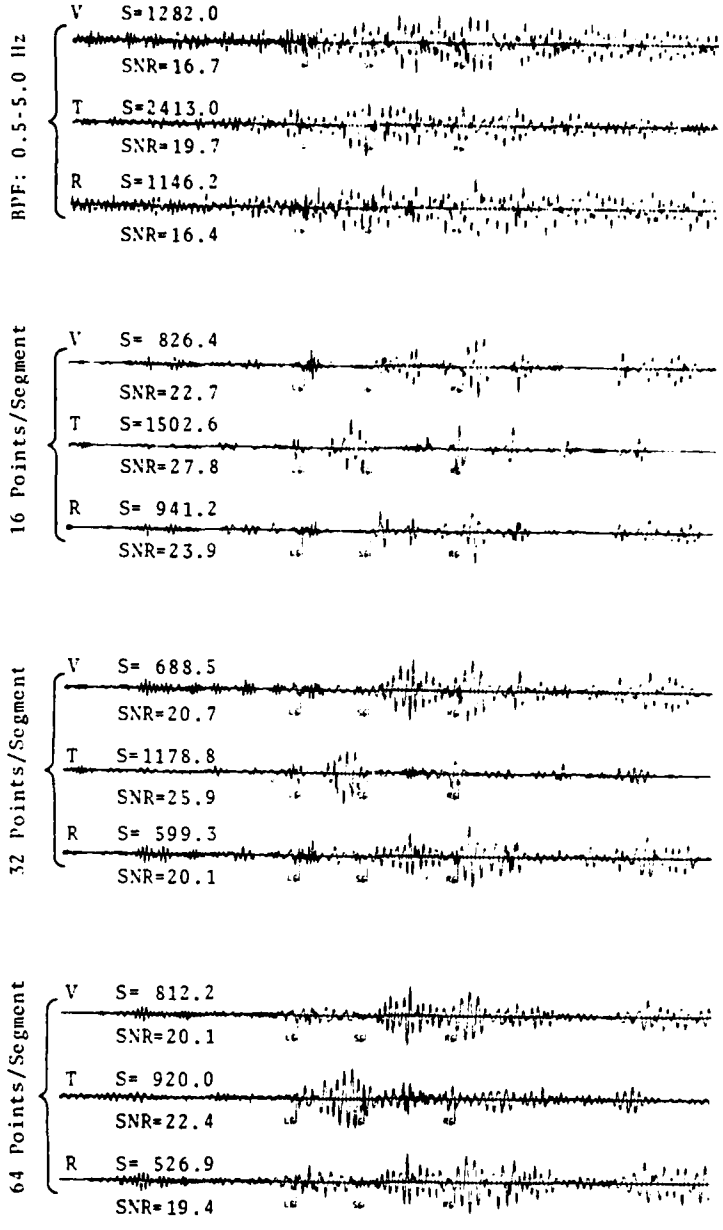

FIGURE II-6

EFFECTS OF CHANGING NUMBER OF POINTS PER PROCESSING SEGMENT ON POLARIZATION FILTER RESULTS

the processing segment increases, in most cases, indicating degradation of the desired signal by interference with noise and the other waveforms in the Lg-Rg window. This result, and that described above, suggest that a segment length of 16 points is preferred.

The choice of the width of the phase pass window, however, is not clear from the results of the data in Table II-2. Though a 10^{o} window width appears to perform better than the other window widths examined, the standard deviation associated with the mean gain values suggest that the mean gain determinations are not statistically different. Therefore, the middle value of the three window widths, 15^{o}, was arbitrarily selected for the phase pass window half-wdith to be used in this work.

In sum, a 16-point time window and a phase window half-width of $\alpha_{o}=15^{o}$ are preferred, and these values were used for all processing described in the remainder of this report. The next section examines the effects produced by the polarization filter on SNR and detection capability.

SECTION III

THE EFFECTS OF POLARIZATION FILTERING ON SIGNAL-TO-NOISE RATIO AND DETECTION CAPABILITY

This section examines the effect of polarization filtering on the signal-to-noise ratios (SNR) of the short-period regional phases and the resulting improvement in detection capability of these phases.

The 'signal buried in noise' technique is used to estimate SNR improvements resulting from polarization filtering. To use this technique, one selects a waveform which has a high SNR and which is preceded by seismic noise. The signal-centered portion of the record is scaled by a factor between zero and '1', and is added to the preceding noise (this process enables the user to control the SNR of data used to test a given signal extraction technique). By varying the scale factor, a suite of three-component composite records can be created covering any desired range in SNR.

The first step toward establishing the SNR gain curve for the polarization filter is to apply the polarization filter to each three-component composite record set. The SNR of each component is measured before and after the filtering process so that the gain due to polarization filtering (i.e., the difference between input and output SNR) can be determined. In computing these SNR values, the point at which the signal amplitude is measured is set to the time of the maximum value of the original signal. This produces SNR measurements which are comparable even at low input SNR values.

To provide an objective measure of input SNR against which to plot the polarization filter gain, a quantity termed 'true input signal-to-noise ratio' is computed. This quantity is defined as follows:

$$\text{TRUE INPUT SNR} = 20 * \text{Log}_{10}\left[\frac{(\text{SF}) * (\text{Max. Amp.})}{\text{RMS Noise}}\right]$$

where

'SF' is the scale factor, and

'Max. Amp.' is the maximum zero-to-peak signal amplitude.

Figure III-1 shows two examples of composite traces formed in the manner described above as they appear before and after polarization filtering. The data were created from a P wave recorded for an event with an epicenter located 8^{o} from the recording site. The true input SNR of Set A is approximately 7 dB while the true input SNR of Set B is approximately 15 dB. The apparent gain in SNR produced by polarization filtering was approximately 8 dB for the data of Set A, and was approximately 12 dB for Set B.

Application of the polarization filter to a suite of data having true input SNR ranging from -4 to 20 dB yields the example of a typical SNR gain curve shown in Figure III-2. In this figure, the polarization filter gain appears to be non-linear for true input SNR values below approximately 14 dB. Above this point, the gain curve flattens, indicating a constant polarization filter gain of 12 dB. This saturation-level gain has, in the past (e.g., Lane, 1973), been taken as the filter gain. The point to be resolved is whether the gain is non-linear below this point.

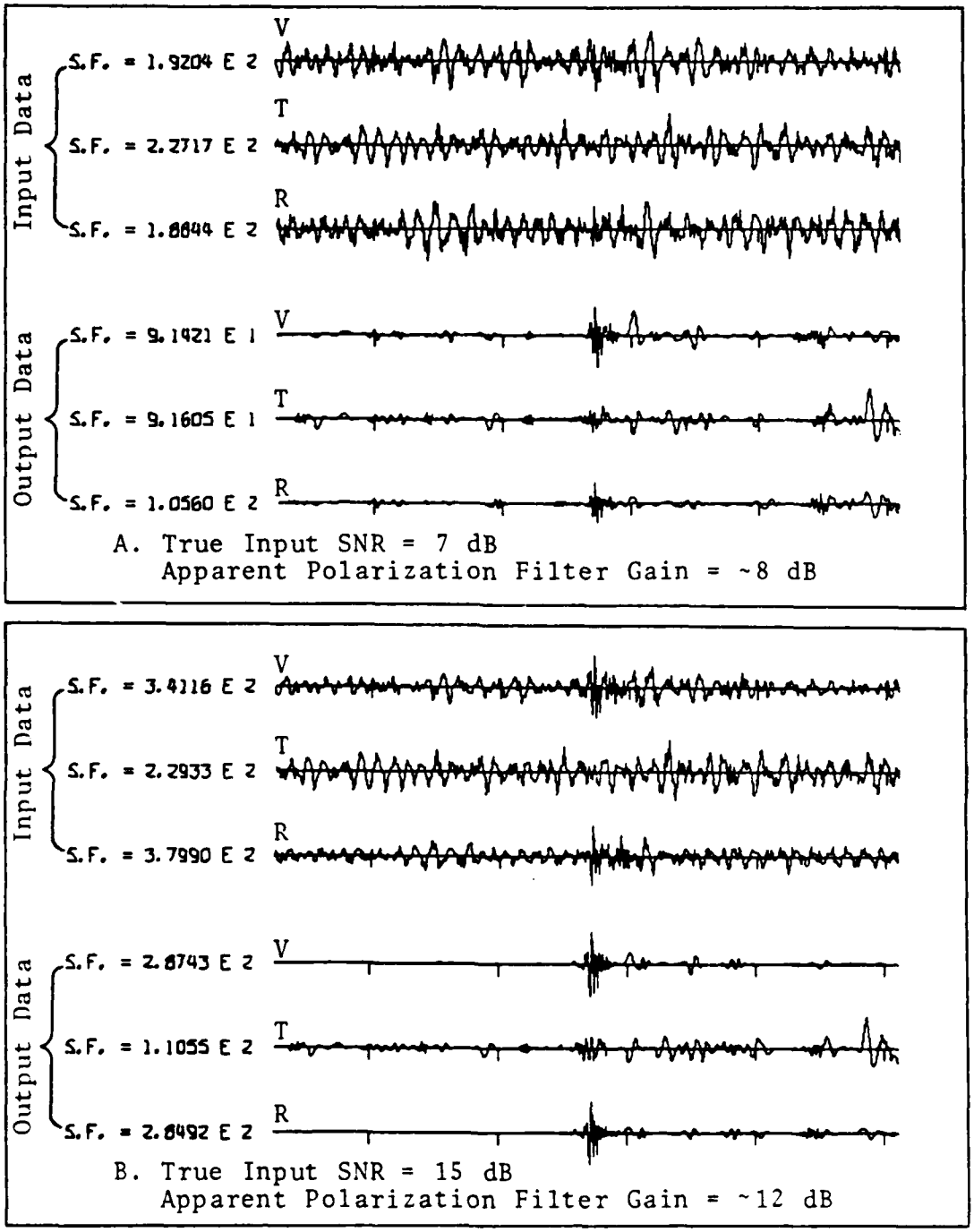

FIGURE III-1

EXAMPLES OF COMPOSITE DATA BEFORE AND AFTER POLARIZATION FILTERING

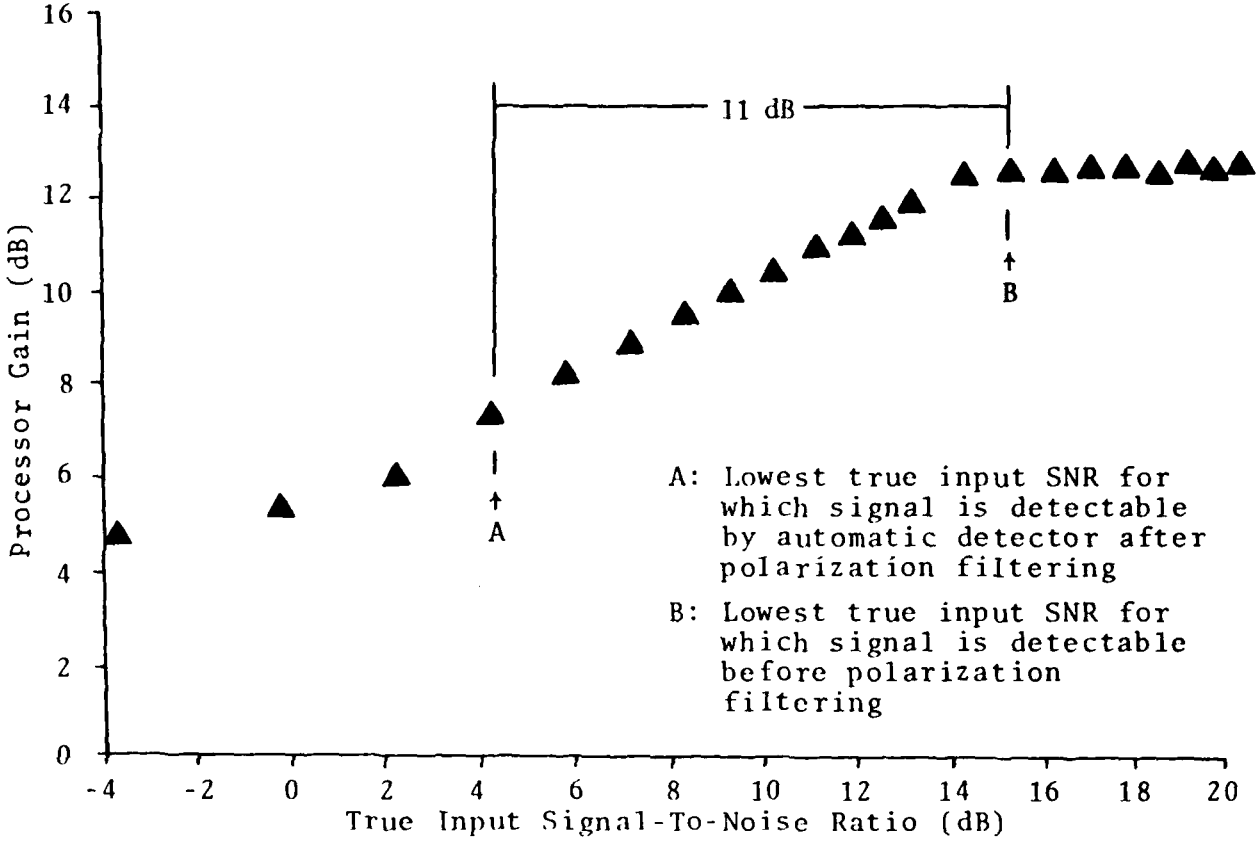

FIGURE III-2

POLARIZATION FILTER GAIN AS A FUNCTION OF TRUE INPUT SIGNAL-TO-NOISE RATIO

This matter of apparent gain non-linearity can be resolved by determining the difference between the true input SNR at which the signal can be detected before polarization filtering and the true input SNR at which the signal can be detected after polarization filtering. To provide an objective estimate of these values of true input SNR, an automatic detector of the type formulated by Unger (1978) was added to the polarization filter program. The results of this detector showed that the gain curve approaches zero slope at about the lowest true input SNR (approximately 15 dB) at which the signal can be detected both before and after polarization filtering. This point is marked by 'B' in Figure III-2. The lowest true input SNR at which the signal can be detected by this automatic detector after polarization filtering, marked by 'A' in Figure III-2, is approximately 4 dB. These results yield a polarization filter gain of 11 dB, which agrees quite well with the previously mentioned value of 12 dB.

This result suggests that the polarization filter gain is constant. An explanation for the apparent non-linear behavior indicated by the data of Figure III-2, however, is that below the lowest true input SNR at which the signal is detected before polarization filtering (Point B), the gain determinations are increasingly influenced by noise. Thus, gain appears to decrease with decreasing true input SNR. This effect is an aberration of the method used to gauge processing gains and, apparently, it does not accurately reflect the performance of the polarization filter.

Figure III-3 shows the polarization filter gain versus true input SNR curves for the Pn, Pg, and regional ($\Delta=12^{o}$) P phases. The curve for Pn was determined from a northeastern

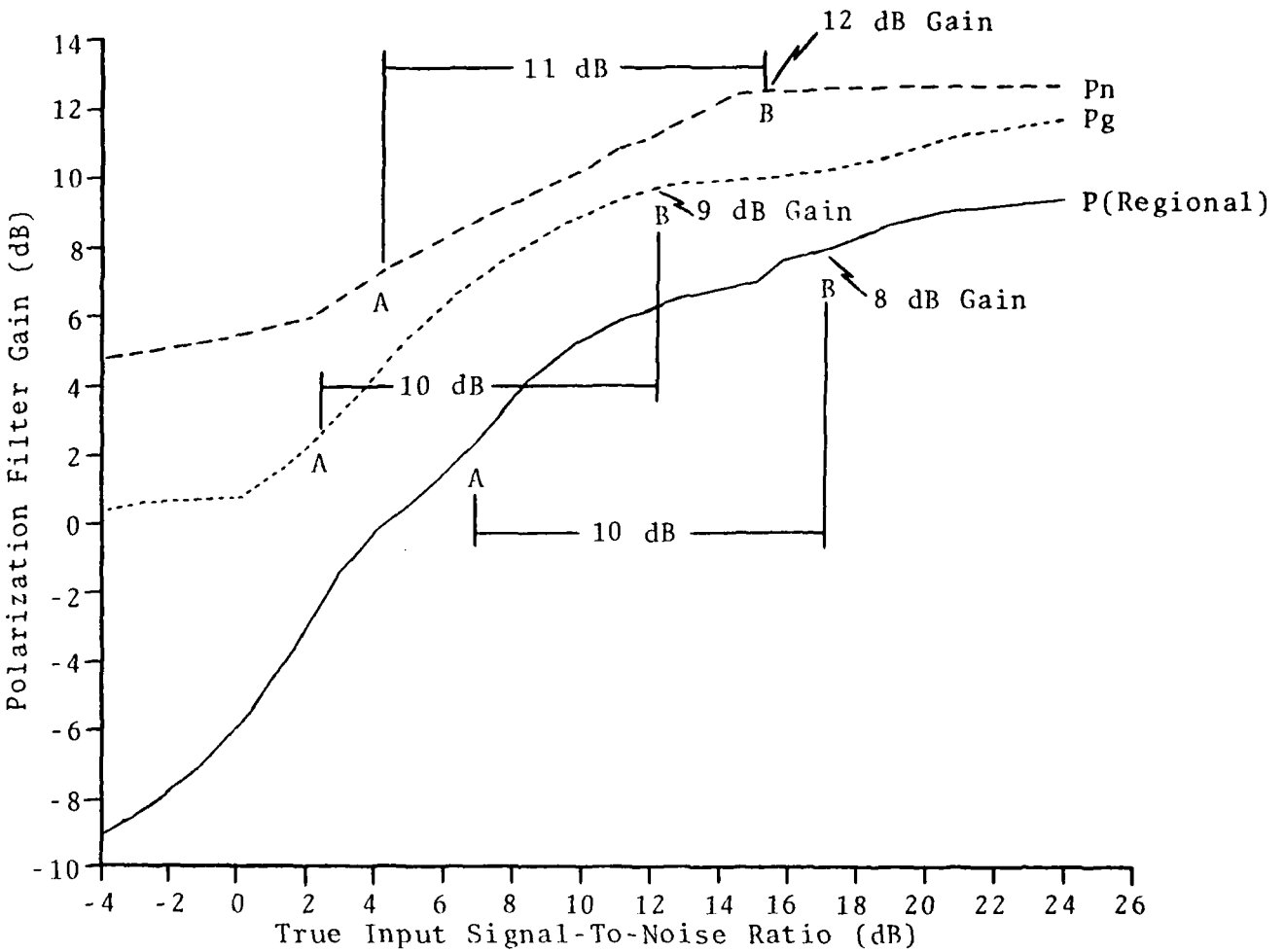

FIGURE III-3

COMPRESSIONAL WAVEFORM POLARIZATION FILTER GAIN CURVES FOR Pg, Pn, AND REGIONAL P

China event, while the curve for Pg was determined from a Kyushu, Japan, event; the curve for regional P was determined from a Honshu, Japan, event. The key data points in this figure are again marked 'A' and 'B'; as before, Point A marks the lowest input SNR for which the automatic detector declared a detection on the polarization filtered data while Point B marks the lowest input SNR for which the automatic detector declared a detection on the bandpass filtered data. These data (i.e., Points A and B) suggest:

- Application of the polarization filter improves the SNR of compressional waves by approximately 10 dB; this implies a lowering of the compressional wave detection threshold of 0.5 m_b units;
- Application of the polarization filter renders detectable a compressional waveform with an SNR as recorded (i.e., 'true') as low as 2-7 dB.

Figure III-4 shows the polarization filter gain versus true input SNR for Sn and regional ($\Delta=12^{o}$) S phases (polarization filter analysis of regional data for the phase Sg presents a special problem which will be discussed later in this section). The curve for Sn was determined from a northeastern China event, while the curve for regional S was determined from a Honshu, Japan, event. The Points A and B on this figure are as previously defined for Figure III-3. These data indicate:

- The polarization filter increases the SNR of shear waves (S or Sn) by approximately 10 dB; this implies a lowering of the shear wave detection threshold of 0.5 m_b units;

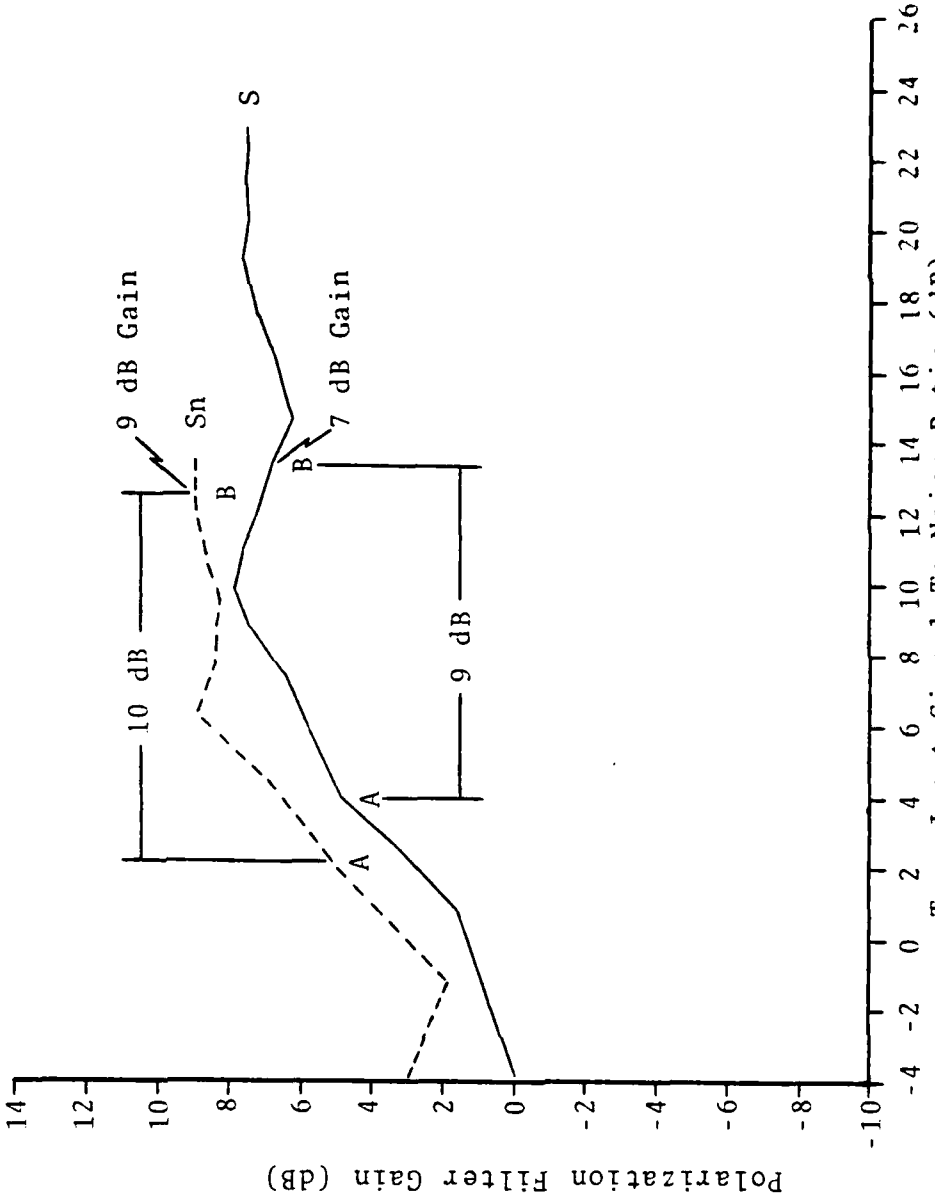

FIGURE III-4

SHEAR WAVEFORM POLARIZATION FILTER GAIN CURVES FOR Sn AND REGIONAL S

- Application of the polarization filter renders detectable a shear waveform with SNR, as recorded, as low as 2-4 dB.

A problem arises when one attempts to determine the effect the polarization filter has on the phases Lg, Rg, and Sg; this is especially true for cases where the event epicenter is at a distance of less than 10^{o} from the recording site. With estimated velocities of 3.5 km/sec for Lg (Ewing, Jardetzky, and Press, 1957), 3.37 km/sec for Sg (Jeffreys and Bullen, 1967), and 3.2 km/sec for Rg, one observes these phases to overlap in time at small epicentral distances (see Figure III-5). This overlap makes it difficult to identify the maximum amplitude of any one of these phases on the bandpass filtered traces. Further, it is not desirable to use the amplitude observed at the predicted phase arrival time since the above-mentioned velocities are not the same everywhere (e.g., Lg velocities as low as 3.2 km/sec have been noted by Herrin and Richmond (1960)). Given the above, estimates of input SNR for Lg, Rg, and Sg will not be reliable, and so, no curves of polarization filter gain versus input SNR are presented for these phases.

Since it was not possible to examine in detail the effect of the polarization filter on SNRs for Lg, Rg, and Sg, as was done for the compressional phases and for the shear phases S and Sn, the polarization filter gain for these phases were estimated in another manner. In particular, a suite of test events showing the overlapping Lg, Sg, and Rg waveforms similar to those shown in Figure III-5 was processed using the shear and surface wave models of the polarization filter. Here, however, the effects of the filter on noise and on the

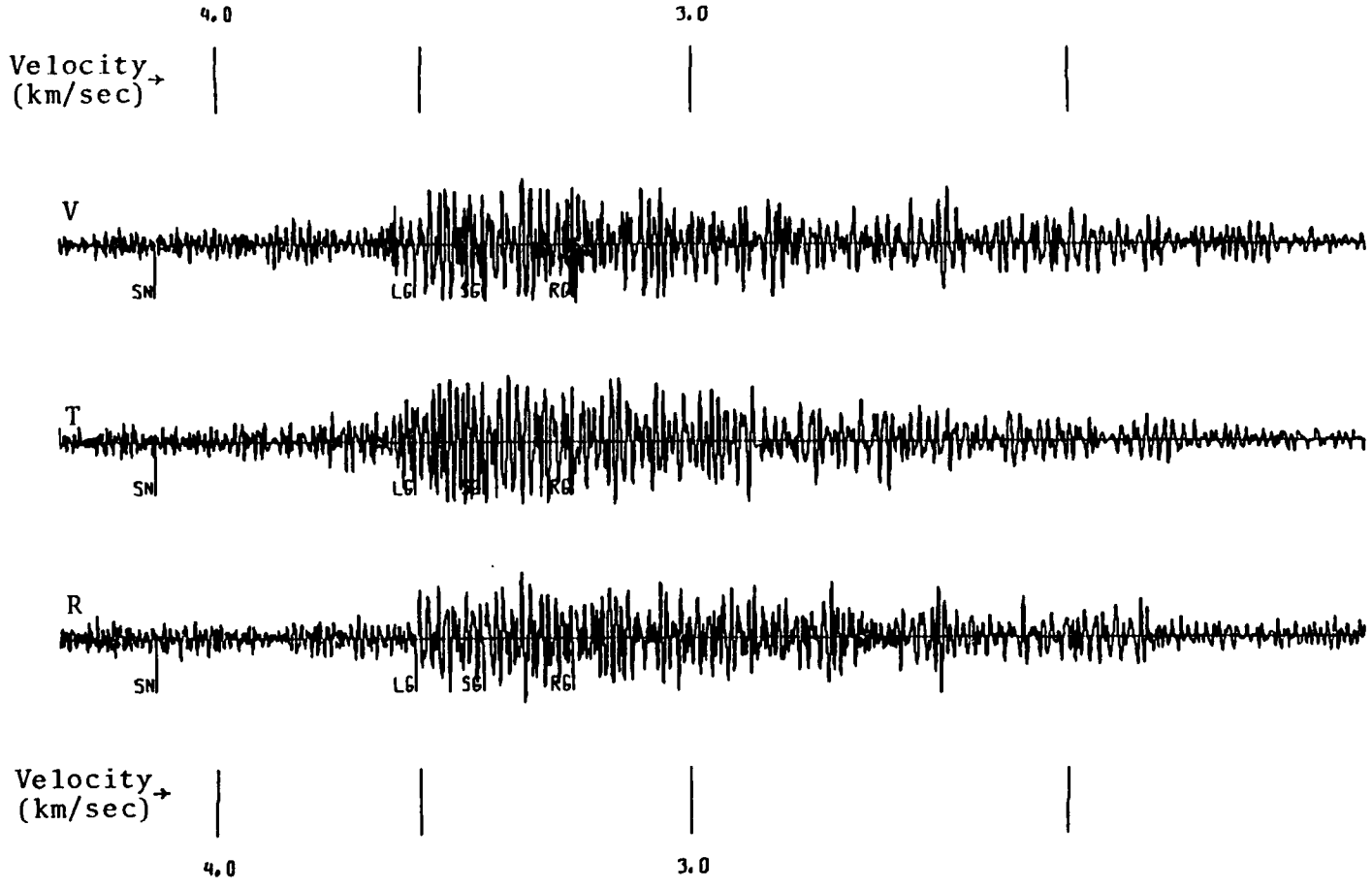

FIGURE III-5

REPRESENTATIVE SAMPLE Lg, Sg, AND Rg WAVEFORMS FOR $\Delta<10^{o}$

signal (as determined by the estimated time of arrival) were determined separately. The difference in the polarization filter's performance on these waveforms, then, is a measure of processor gain. Suites of compressional and shear data were also processed in the same manner so as to provide gain estimates which could be compared to those previously determined.

The results of this analysis effort are summarized in Table III-1. The table gives the sample population means in dB (plus-or-minus one standard deviation) for the degree of noise suppression, the degree of signal suppression, and the estimated gain in SNR produced by polarization filtering. The polarization filter gains for Sg, Lg, and Rg are 13 dB, 8 dB, and 8 dB, respectively. It is of interest to note that gains in SNR produced by the polarization filter for the compressional and shear (S and Sn) phases as determined by this method agree well with the gains determined earlier by the signal-buried-in-noise method (i.e., gains ~10 dB), thereby lending credence to the method used to measure the processor gains determined for Sg, Lg, and Rg.

The SNR gains of Table III-1 imply increases in the detection threshold of 0.5 m_b units for compressional and shear (S, Sn) waves, 0.6 m_b units for Sg, and 0.4 m_b units for Lg and Rg.

Confirmation of the detection threshold results is sought by making direct estimates of the detection thresholds before and after application of the polarization filter. The data available for this work, however, only allowed computation of direct estimates of the detection thresholds for regional P

TABLE III-1

EFFECTS OF POLARIZATION FILTER ON THE SIGNAL-TO-NOISE RATIOS OF REGIONAL PHASES

Phase	Noise Suppression (dB)	Signal Suppression (dB)	Net Gain (dB)
Sg	16.8 ± 3.5	4.0 ± 3.6	12.8 ± 5.4
Lg	10.4 ± 1.8	2.6 ± 1.8	7.9 ± 2.2
Rg	12.1 ± 2.7	4.0 ± 1.6	8.1 ± 3.0
P, Pn	14.0 ± 3.2	3.6 ± 1.8	10.4 ± 3.4
S, Sn	16.6 ± 4.3	6.0 ± 4.4	10.5 ± 6.0

Values shown are sample population means in dB (plus-or-minus one standard deviation).

and regional S; insufficient data were available to make these estimates for Pn, Pg, Sg, and Sg. Of the approximately 340 events studied, only about 40 had epicentral distances such that these phases might have been detected. However, a group of 123 P waves and 120 S waves from events in the Honshu and Hokkaido, Japan, areas (epicentral distances = 10^{o} to 13^{o}) were available for direct estimates of detection capability for regional P and S. Unfortunately, these could not also be used for Lg and Rg since the Sea of Japan, which lies between the source and the receiver, blocks transmission of Lg (and perhaps Rg, as well, as no Rg was observed on any of these records). This situation is to be expected since Ewing, Jardetzky, and Press (1957) note that as little as 2^{o} of ocean crust between source and receiver will block transmission of Lg. Thus, it is possible to make direct estimates of detection capability thresholds only for regional P and S. These should, however, suffice to confirm or deny the previously stated changes in detection threshold determined from the computed signal-to-noise ratio gains.

The method used for making direct estimates of detection capability is to examine visually the data traces recorded for each event after bandpass filtering and again after polarization filtering in order to determine whether the waveform is detectable. Statistics of the detection status for the events of the data base were then compiled and were used to compute the percentages of events detected at each bodywave magnitude increment (bodywave magnitudes are those reported by the National Earthquake Information Service). The cumulative Gaussian probability function is then fitted to these detection percentage statistics by the maximum likelihood method formulated by Ringdal (1974).

Detection threshold results are presented in Figures III-6 (for P waves) and III-7 (for S waves). Figures III-6A and III-7A show the results for the data after bandpass filtering but before application of the polarization filter; Figures III-6B and III-7B show the results for the data after polarization filtering. The upper portion of each figure shows the number of detections and non-detections at each bodywave magnitude increment; the lower portion shows the resulting detection percentages and the fitted Gaussian probability function. The statistic on which the before and after polarization filtering comparison is made is the 50 percent detection threshold, denoted by 'm_b50' in these figures. Comparison of the m_b50 values shows a lowering of the detection threshold of 0.59 m_b units for P waves and 0.5[illegible] m_b units for S waves. These values compare well with the detection threshold improvements determined using the 'signal-buried-in-noise' method (0.5 m_b units in both cases).

In summation, the data indicate that the polarization filter may be expected to improve the detection capability of a three-component short-period station by approximately 0.5 to 0.6 m_b units for Pn, Pg, and regional P, by approximately 0.5 to 0.6 m_b units for Sn, Sg, and regional S, and by approximately 0.4 m_b units for Lg and Rg.

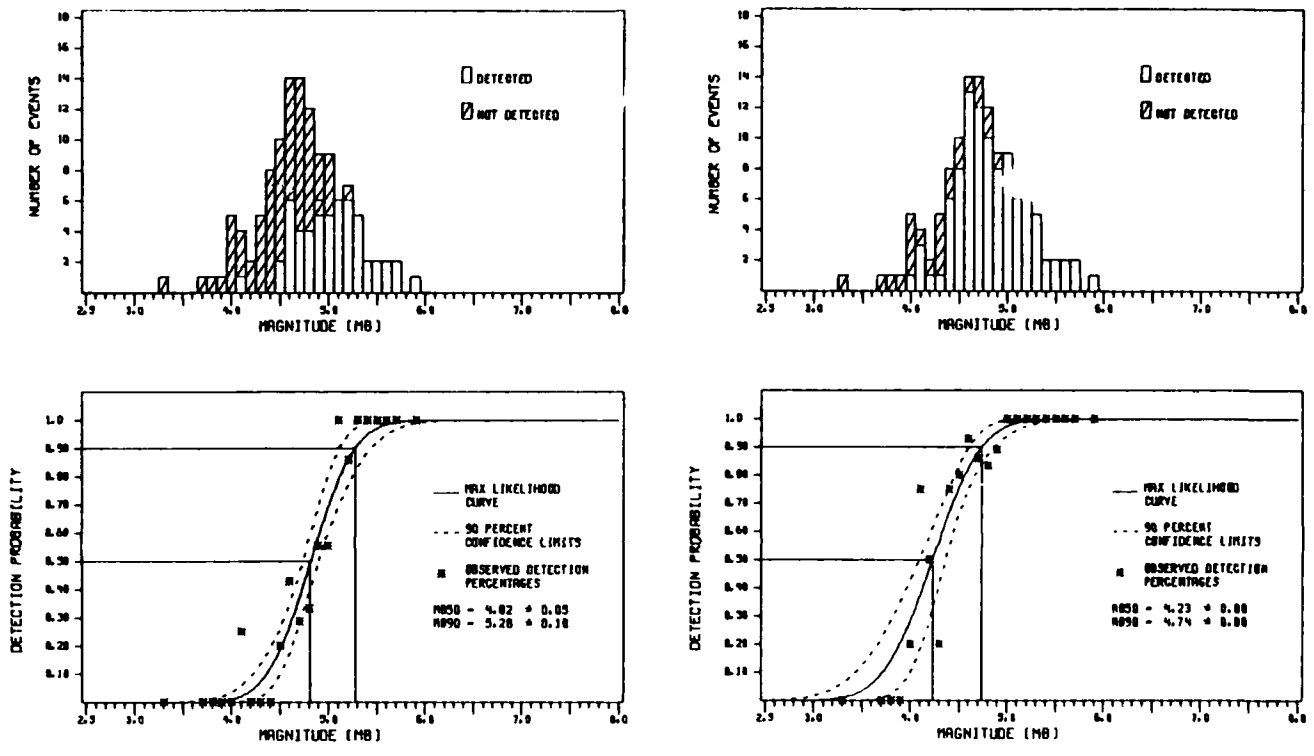

A. P-Wave Detection Statistics Before Polarization Filtering

B. P-Wave Detection Statistics After Polarization Filtering

FIGURE III-6

P-WAVE DETECTION STATISTICS

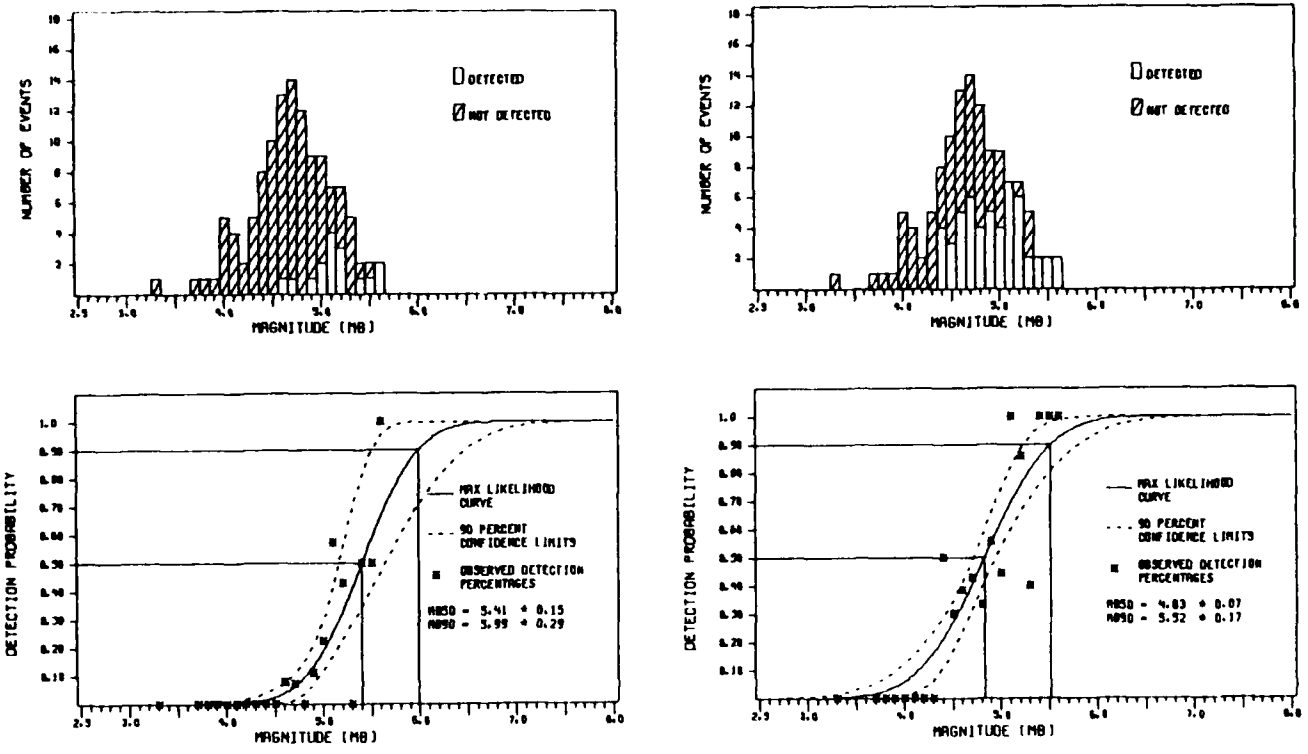

A. S-Wave Detection Statistics Before Polarization Filtering

B. S-Wave Detection Statistics After Polarization Filtering

FIGURE III-7
S-WAVE DETECTION STATISTICS

SECTION IV
EXAMPLES OF POLARIZATION FILTER USAGE

This section presents examples of polarization filtered data. These examples were selected to demonstrate the value of this filter in the areas of signal extraction, signal identification, and mixed signal separation. In each figure in this section, the notations to the left of each set of traces denote the following:

- BPF - the bandpass-filtered data which were input to the polarization filter program (0.5-5.0 Hz passband unless otherwise specified)
- P - the data output by the compressicnal model of the polarization filter
- Lg,Rg - the data output by the retrograde elliptical model of the polarization filter and the transverse component Lg algorithm
- S - the data output by the shear model of the polarization filter.

The letters V, T, R indicate the vertical, transverse, and radial components of motion, respectively. The notation 'S='(some number) indicates the maximum amplitude of the trace in digital counts. The tick marks labeled P, Pn, Pg, S, Sn, Sg, Lg, or Rg indicate the predicted arrival time of the designated phase. When a symbol of the type Pn↓ appears above a trace, it indicates a visually picked phase arrival of the type named in the symbol.

Figure IV-1 illustrates the extraction of Pn and Pg from a record with low SNR. Figure IV-1A shows the results of applying the compressional model of the polarization filter to data which were preprocessed with the standard 0.5-5.0 Hz bandpass filter. In the bandpass-filtered data, it is barely possible to detect the Pn arrival, while the Pg arrival is not detectable. After polarization filtering, the Pn and Pg phases are visually detectable, as indicated. Figure IV-1B is presented to show the improvement which can be achieved by using narrowband bandpass filter (1.25-5.0 Hz) as a preprocessor to the polarization filter when the dominant frequency of the sought-after phases can be estimated. These results serve to demonstrate that interactive processing, with its ease of selection of time gates and program parameters, is more suitable for polarization filter application than is the batch processing environment.

A second example of regional waveform extraction is shown in Figure IV-2. The bandpass-filtered traces at the top of the figure show P-coda, decaying from left to right, which extend into and overlap onto the (presumed) Sn arrival which arrives approximately 15 seconds before the predicted Sn arrival time. The problem presented by these data is twofold: (1) without source-to-station calibration, one cannot be certain that the waveform observed at the predicted arrival time for Sn is, indeed, Sn; (2) if the phase observed is Sn, there is a question as to where the phase starts. Application of the shear model of the polarization filter resolves these questions as seen in the lower set of traces; the start time for Sn is easily determined, and further, the phase can be identified with confidence as a shear phase on the basis of its being passed by the shear model.

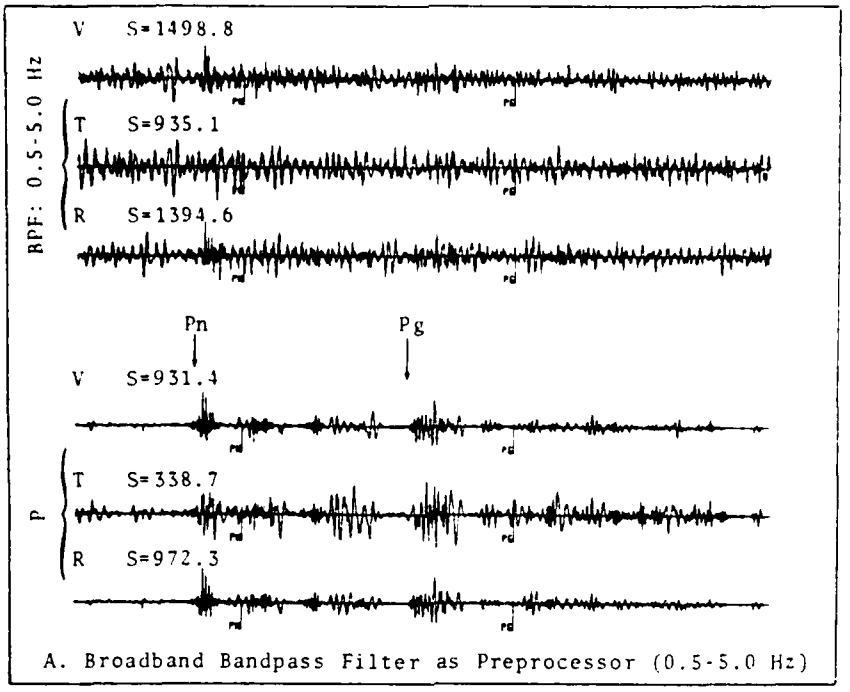

A. Broadband Bandpass Filter as Preprocessor (0.5-5.0 Hz)

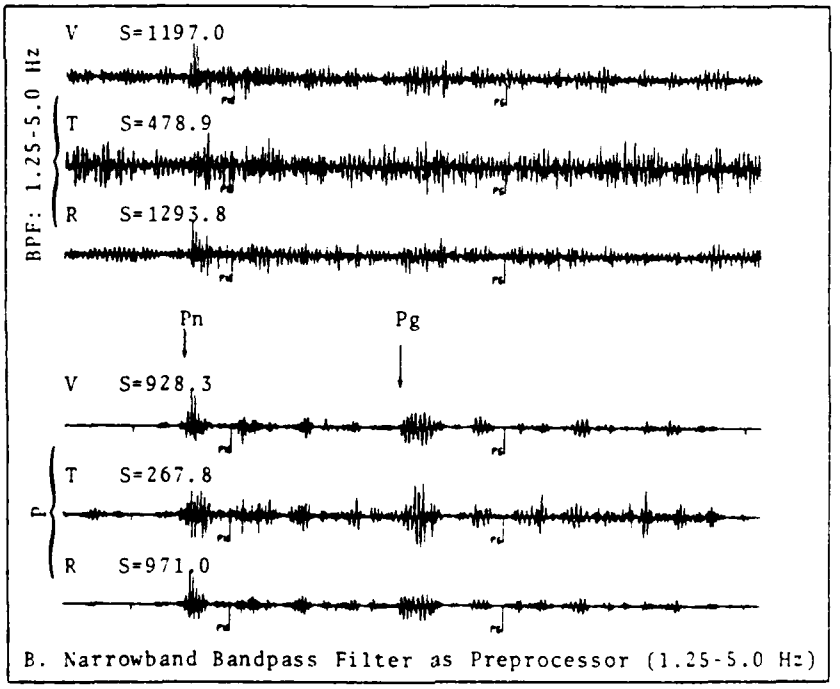

B. Narrowband Bandpass Filter as Preprocessor (1.25-5.0 Hz)

FIGURE IV-1
EXTRACTION OF Pn AND Pg PHASES

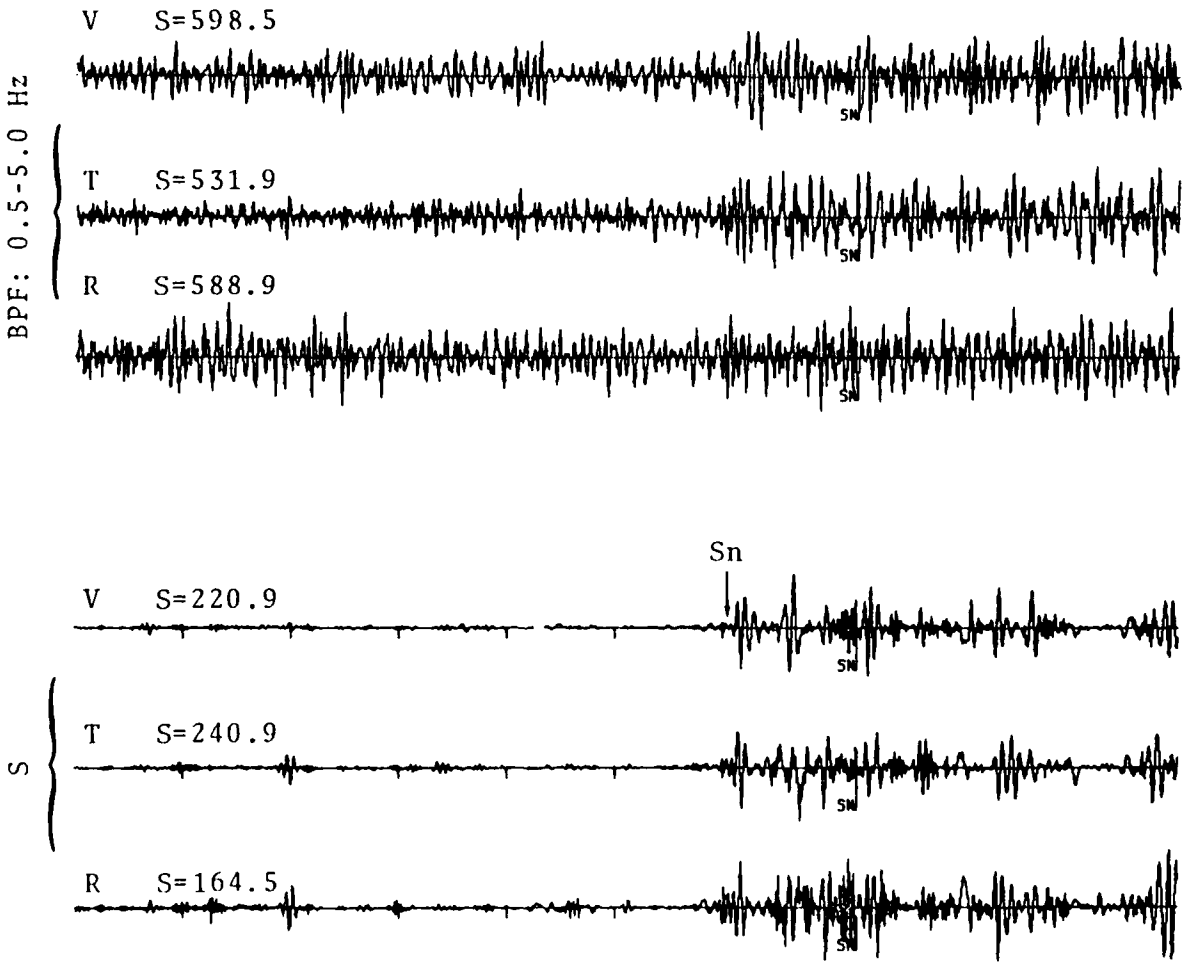

FIGURE IV-2
EXTRACTION OF Sn FROM P-CODA AND SEISMIC NOISE

A third example of regional waveform extraction is shown in Figure IV-3. The bandpass-filtered traces at the top of the figure show shear (Sn) coda extending into, and mixing with, waveforms which presumably are Lg, Sg, and Rg. As with the data shown in the previous figure, the problem here is to determine whether Lg, Sg, and Rg can be identified, and whether their start times can be determined. The second set of traces in Figure IV-3 shows the result of applying the shear model of the polarization filter to the bandpass-filtered data. The shear phase Sg can now easily be identified, and its start time is easily determined. The third set of traces in Figure IV-3 shows the results of applying the retrograde elliptical model of the polarization filter and the Love wave extraction algorithm to the bandpass-filtered data. The Rg phase can now be identified and its start time can be determined on the vertical and radial traces. On the transverse trace, Lg is clearly visible.

Figure IV-4 shows a somewhat different extraction problem which must be resolved. Here, the Pn arrival is so large that is completely masks later arrivals. Application of the compressional model of the polarization filter strips away the Pn coda, revealing the Pg arrival. There is an apparent compressional arrival between Pn and Pg revealed by the polarization filter. The origin of this arrival is at present unknown and should be investigated. This arrival typifies one of the uses of the polarization filter — to extract waveforms not previously seen due to masking coda.

Figure IV-5 is presented to illustrate the effects of the polarization filter on coda. The P wave shown in this figure was generated by an event with an epicentral distance

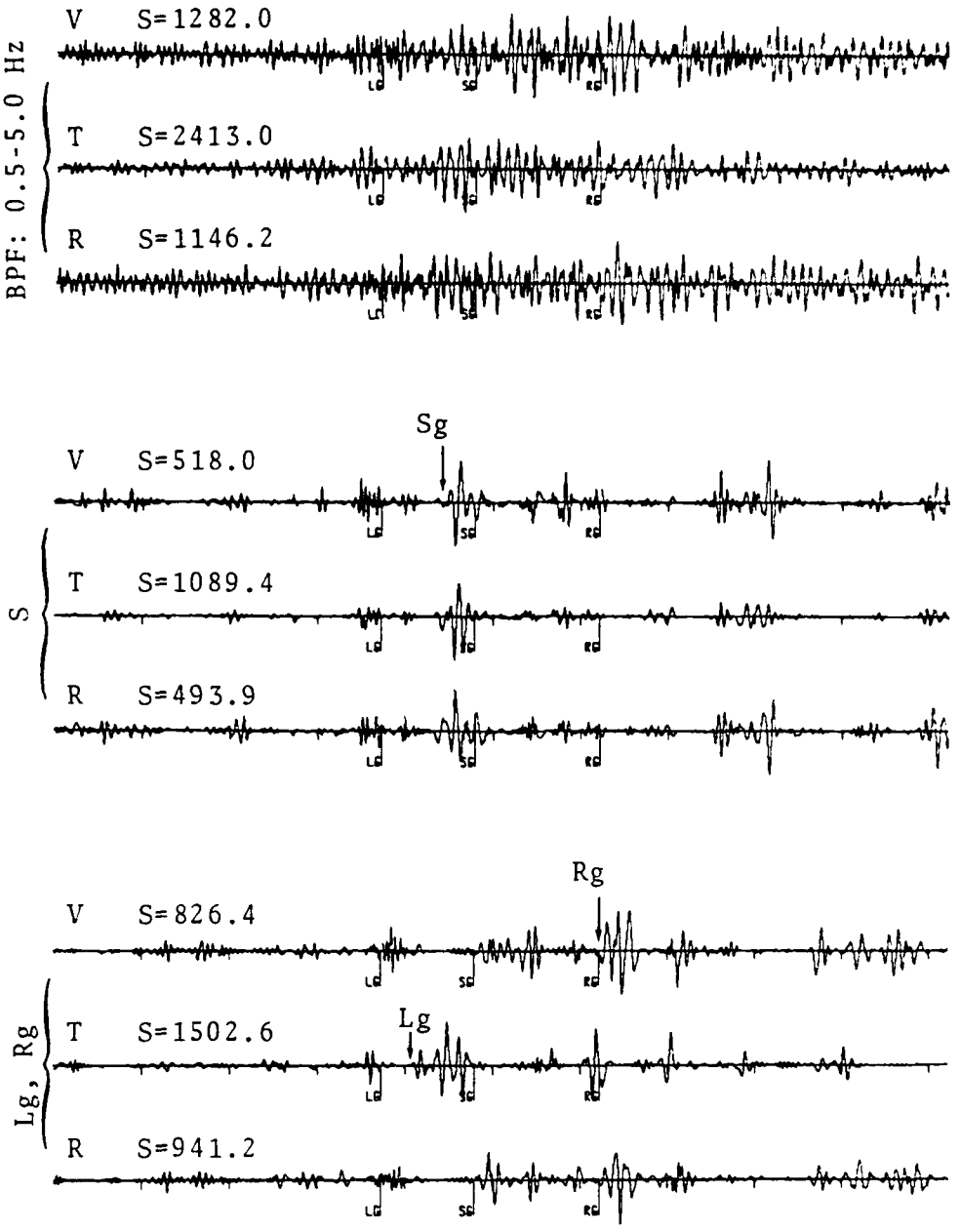

FIGURE IV-3

EXTRACTION OF Sg, Lg, AND Rg FROM SHEAR CODA AND SEISMIC NOISE

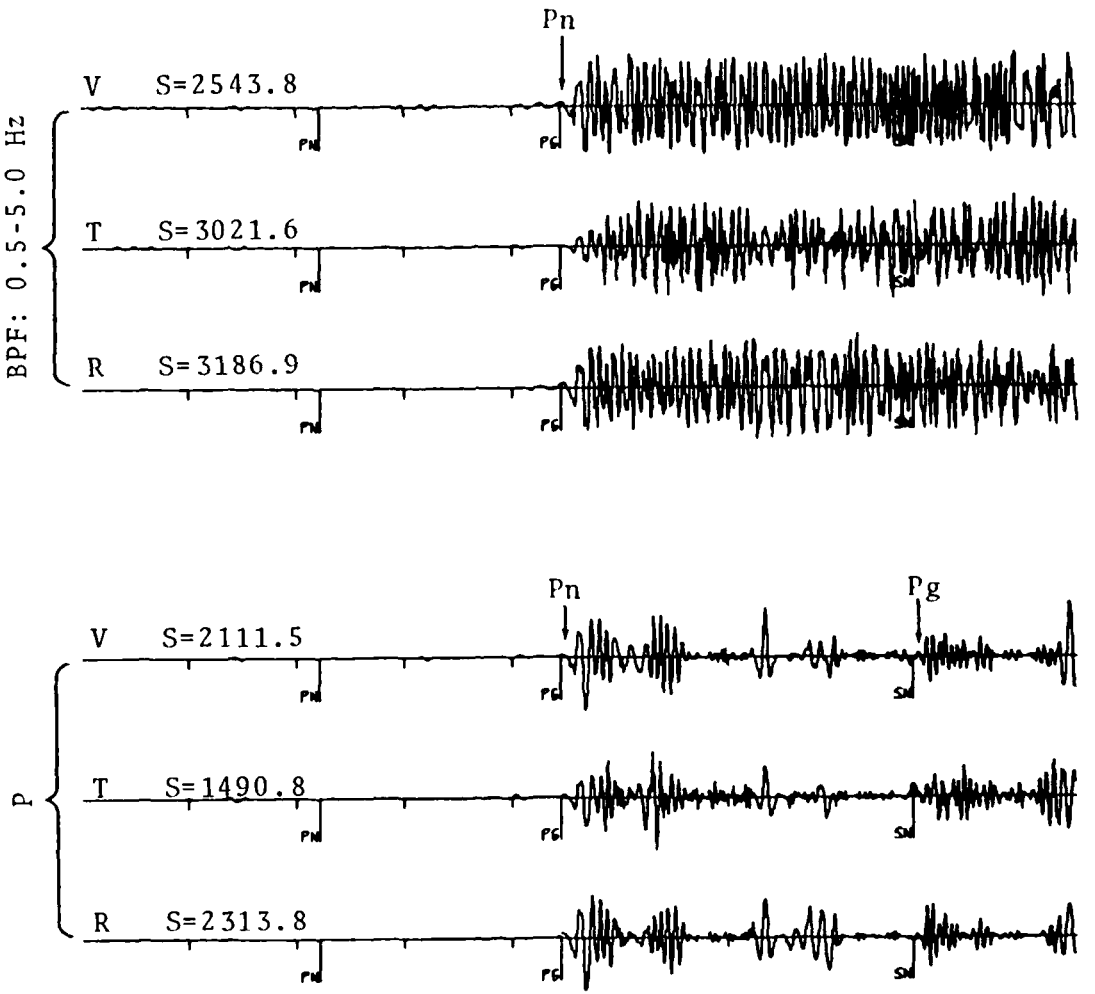

FIGURE IV-4
EXTRACTION OF Pg FROM Pn-CODA

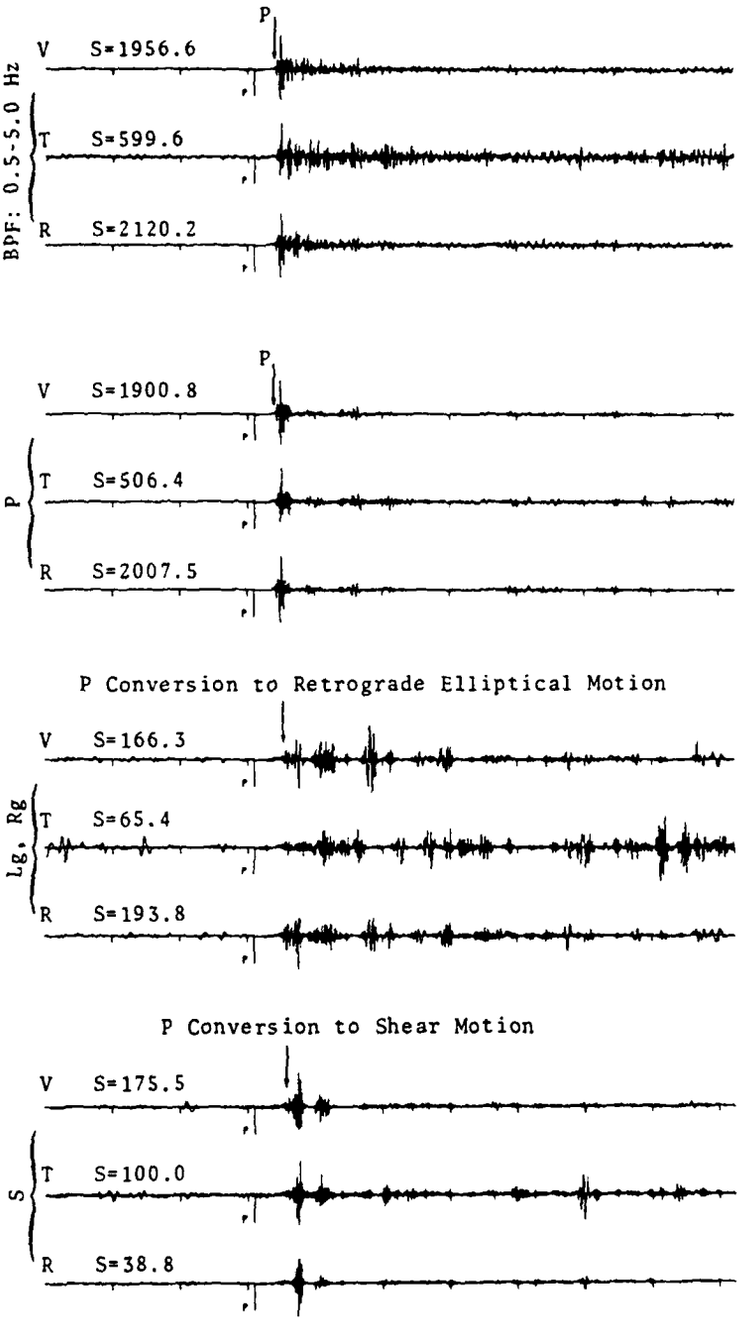

FIGURE IV-5
P CONVERSION TO OTHER PROPAGATION MODES

of approximately 9^{o} and with a crustal travel path. The top set of traces shows the bandpass-filtered data while the subsequent sets show the traces produced by application of the compressional, retrograde elliptical, and shear models, respectively. After application of the compressional model, the P coda is almost completely suppressed while the maximum amplitudes of the first arrivals on the vertical and radial components are reduced less than five percent. Application of the retrograde elliptical and shear model show that the P coda suppressed by the compressional model exhibit retrograde elliptical and shear mode characteristics. This suggests that P conversion to these modes is taking place near the free surface. Note that the waveforms on the retrograde elliptical and shear model filtered traces have amplitudes approximately one-tenth of the waveforms passed by the compressional model.

Figures IV-6 and IV-7 illustrate another important interpretation of polarization filter signal extractions. Figure IV-6 shows the P time gate of a presumed Honshu, Japan, event with a reported epicentral distance of 11^{o}; Figure IV-7 shows the S time gate for the same event. Application of the compressional model of the polarization filter to the P time gate shows that the P arrival actually consists of an emergent Pn arrival (arrival time uncertain) and an impulsive Pg arrival. Application of the compressional model of the polarization filter to the S time gate shows that the purported S arrival for this event actually consists of two compressional waveforms from a second event (note phases tentatively identified as Pn(2) and Pg(2) in Figure IV-7). The low amplitude arrival near the start of the S time gate passes as a shear wave (Sn of Figure IV-7). Thus, this reported Honshu

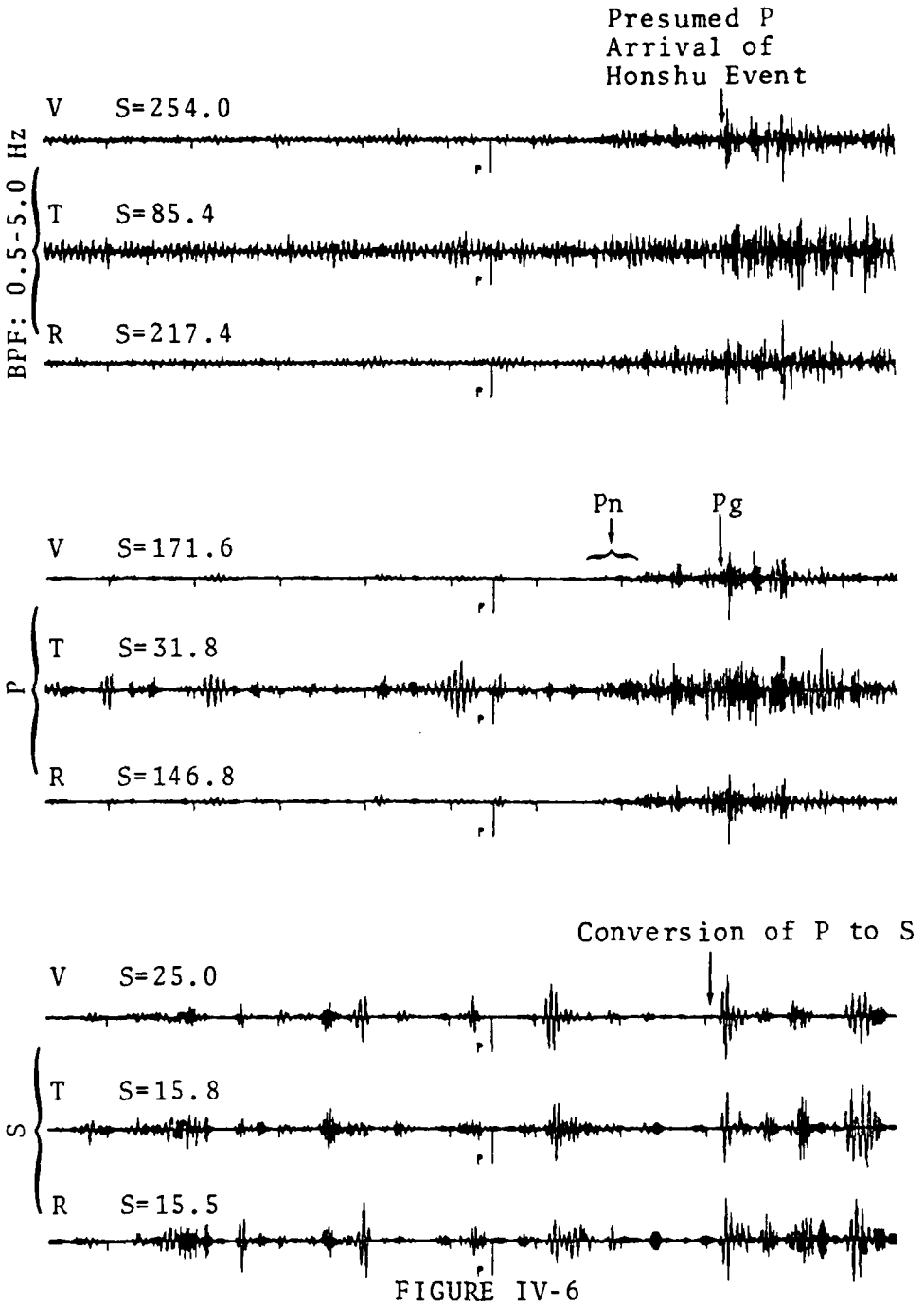

FIGURE IV-6

P GATE OF REPORTED HONSHU, JAPAN EVENT

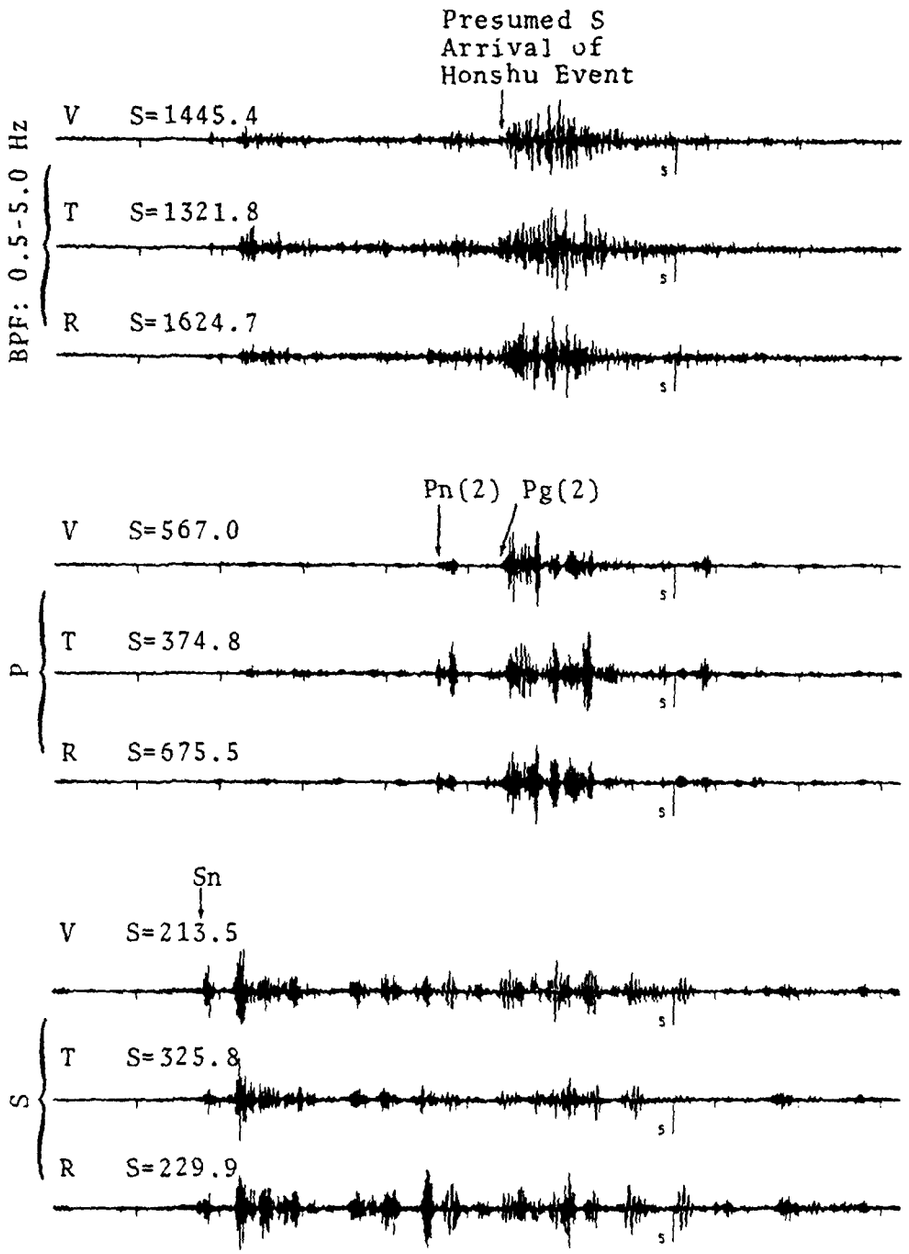

FIGURE IV-7
S GATE OF REPORTED HONSHU, JAPAN EVENT

'event' appears, actually, to be two events; the first had an epicentral distance of 4^{o}-5^{o} (based on the Pg, Sn arrival time difference) while the second had an epicentral distance of 3^{o}-4^{o} (based on the Pn(2), Pg(2) arrival time difference). These results demonstrate that the polarization filter can be used to identify phases with more confidence, and can result in improved event location and measurement capabilities.

The remaining four figures, Figures IV-8, IV-9, IV-10, and IV-11, illustrate the results of applying the polarization filter to mixed signals. Figure IV-8 presents the bandpass-filtered vertical, transverse, and radial traces for an event in northeastern China with an epicentral distance of 8^{o} (for clarity, the second half of the data window is presented below the first half). To the left of the P tick mark in this figure is seen the coda of an earlier event (presumably consisting of the Lg and Rg phases). The first arrival of the selected event can be seen just to the right of the P tick mark. A small increase in amplitude just to the left of the Sn tick mark may indeed be this phase. Another arrival can be seen between the Sn and Lg tick marks. Following this is the Lg, Sg, and Rg train of waveforms. The amplitude increase near the end of the record may mark the arrival of another such wavetrain. To resolve and identify these various arrivals, the polarization filter was applied to the three time gates marked in Figure IV-8.

Figure IV-9 presents the results of applying the polarization filter to the data in the P time gate of Figure IV-8. The coda to the left of the signal is stripped away by the compressional model, leaving the clearly defined arrivals Pn(1) and Pg(1). The coda removed by the compressional model appears

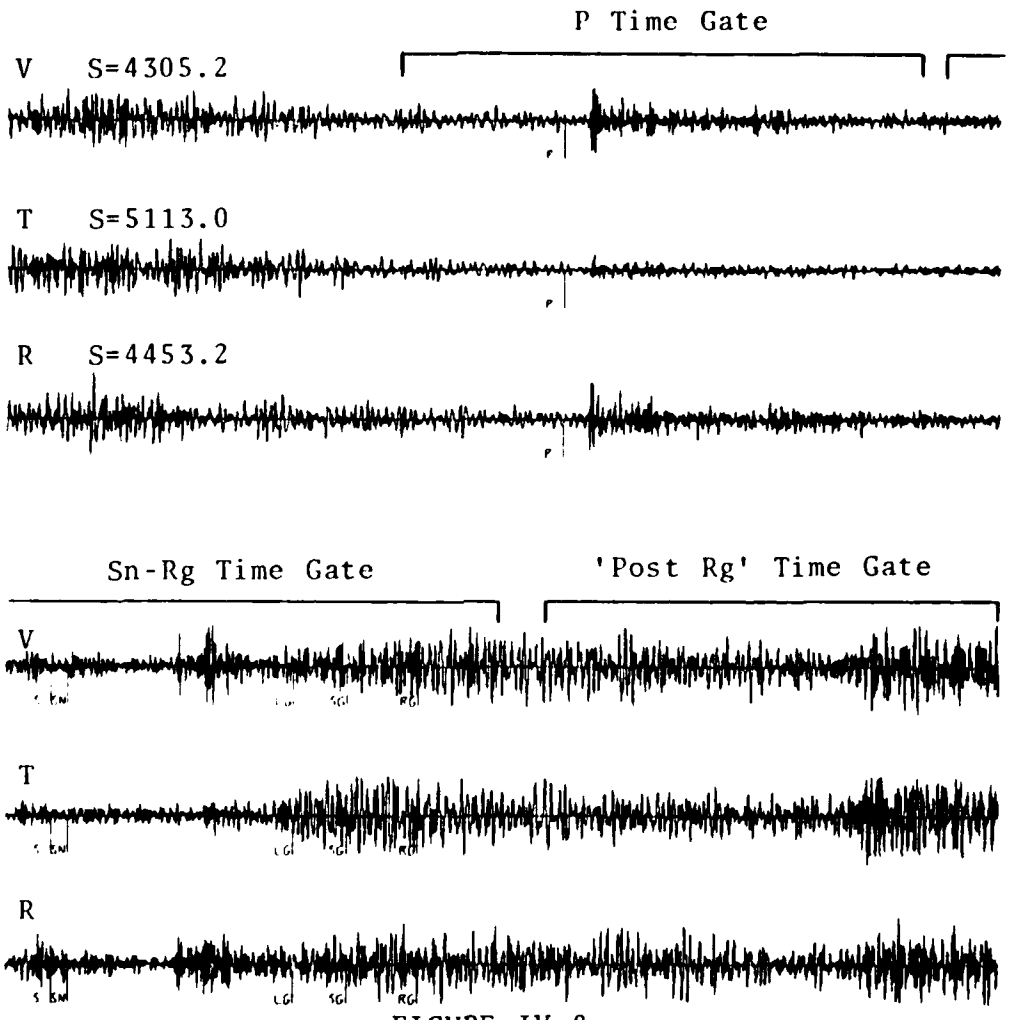

FIGURE IV-8

DATA FOR MIXED SIGNAL SEPARATION

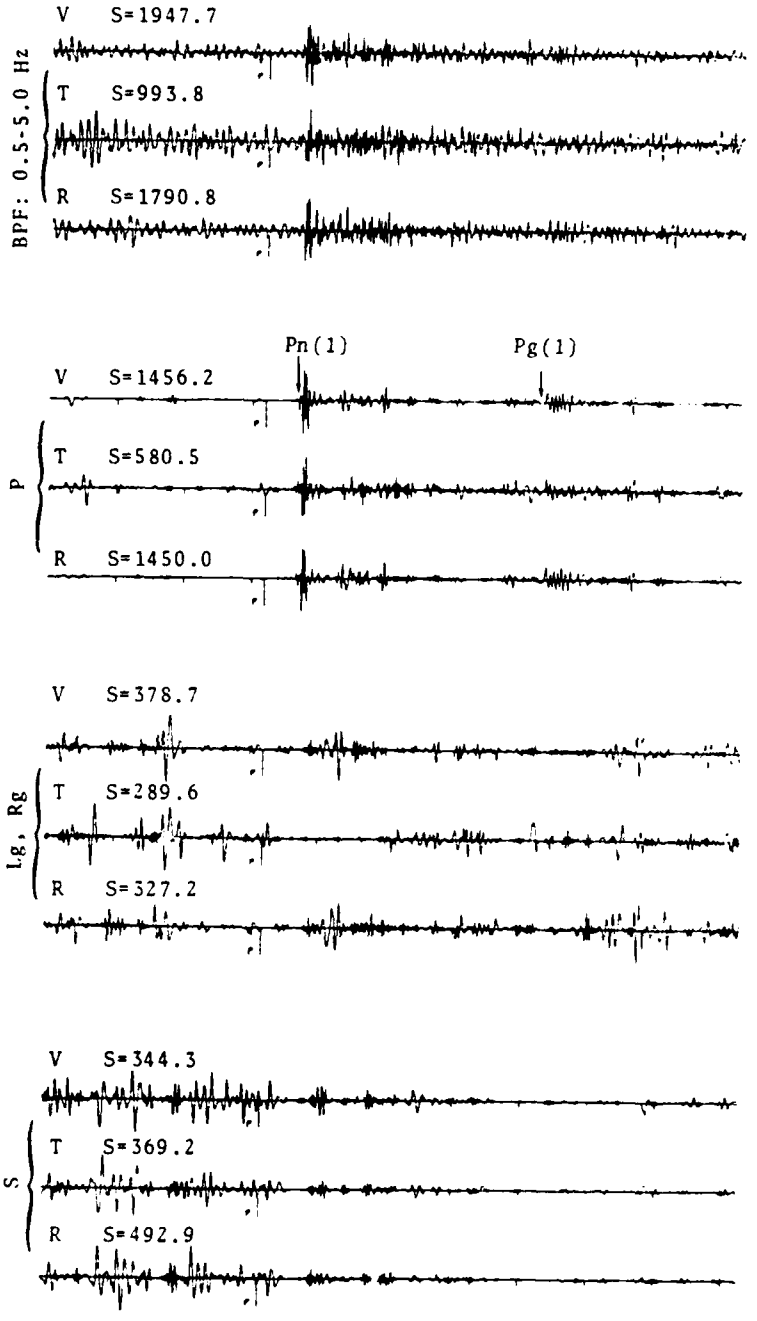

FIGURE IV-9
P GATE OF EVENT OF FIGURE IV-8

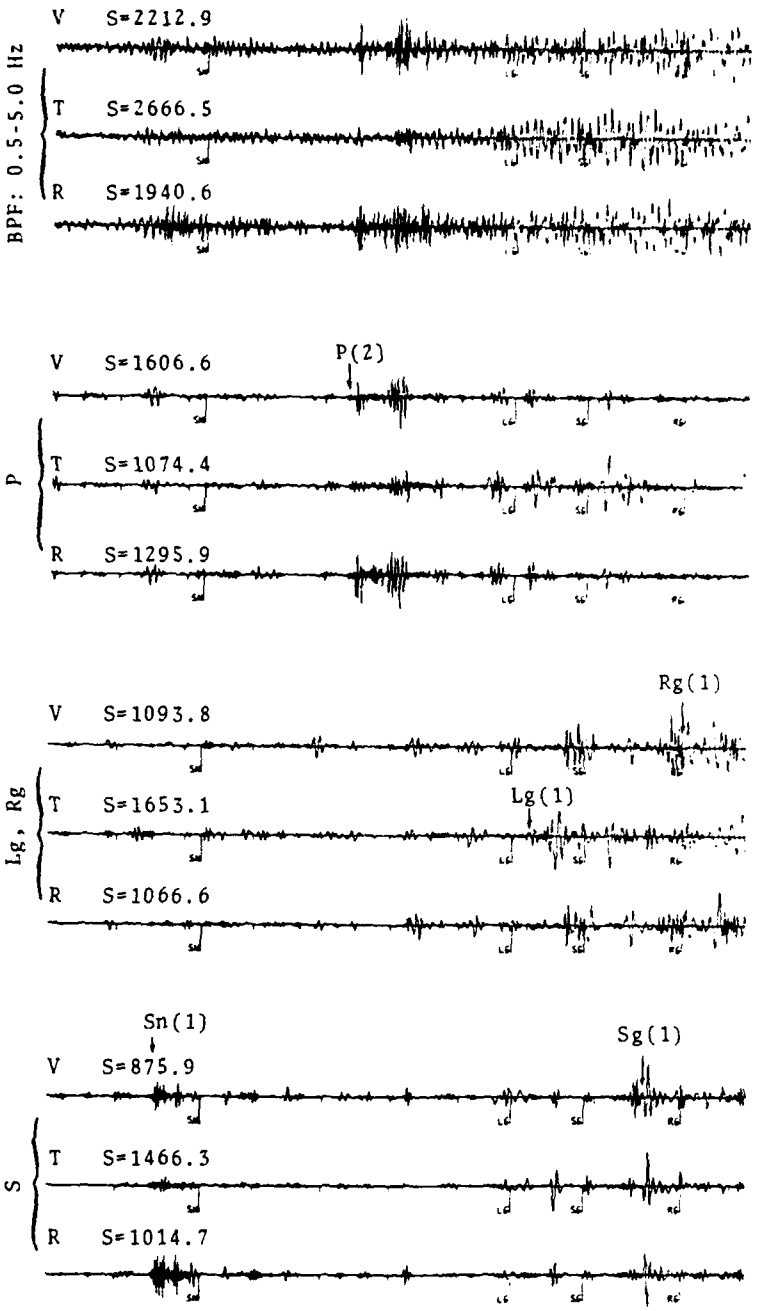

FIGURE IV-10
Sn-Rg GATE OF EVENT OF FIGURE IV-8

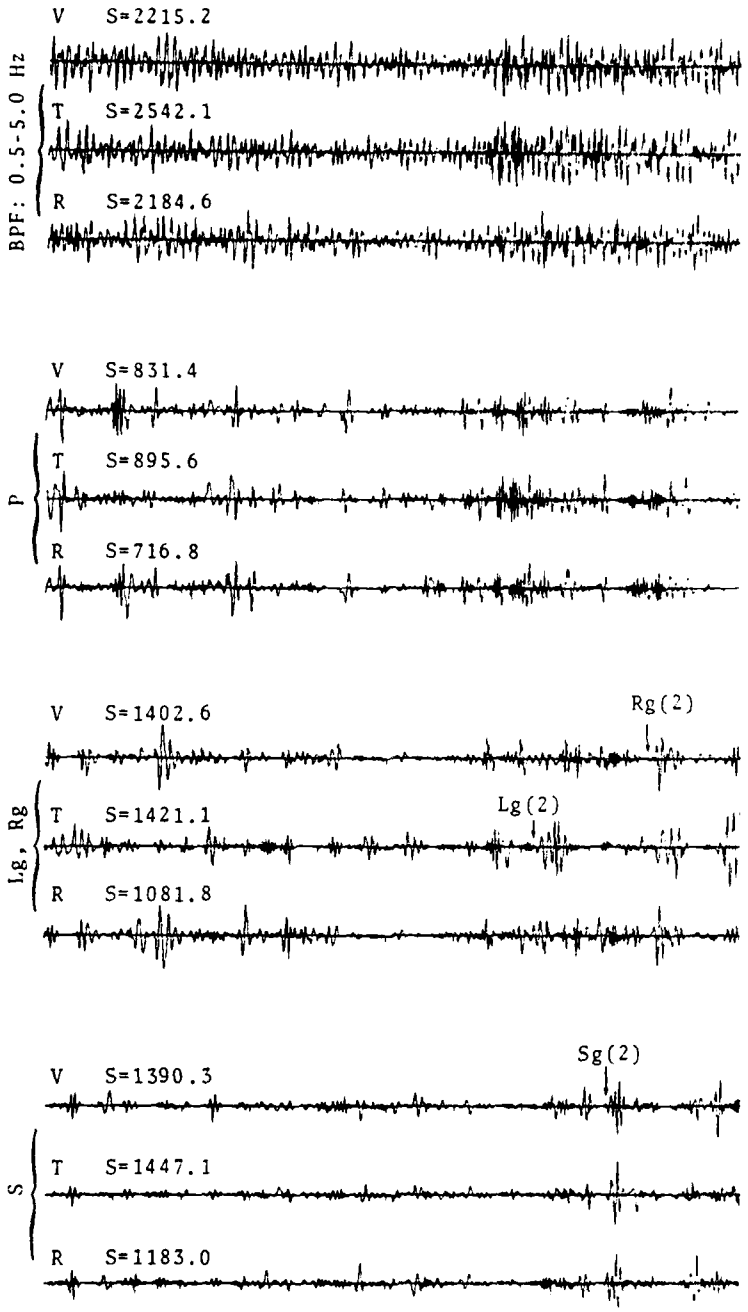

FIGURE IV-11

POST-Lg,Rg GATE OF EVENT OF FIGURE IV-8

on the output from the retrograde elliptical and shear models, thereby indicating that this coda is the Lg, Sg, and Rg wavetrain of an earlier event.

Figure IV-10 presents the results of applying the polarization filter to the data in the Sn-Rg time gate of Figure IV-8. The output from the compressional model clearly identifies the waveform located between the Sn and Lg tick marks as a P wave (identified as P(2) in Figure IV-10). Also indicated on the appropriate traces in this figure are the Sn, Sg, Lg, and Rg arrivals associated with Pn(1) and Pg(1) of Figure IV-9.

Finally, Figure IV-11 presents the results of applying the polarization filter to the data in the 'Post-Rg' time gate of Figure IV-8. These data show that the second wavetrain of Figure IV-8 consists of the overlapping Lg, Sg, and Rg waveforms which can be associated with arrival P(2) of Figure IV-10. These arrivals, indicated by Lg(2), Sg(2), and Rg(2), are marked on the appropriate traces.

In sum, this section has illustrated the value of the polarization filter in extracting short-period regional phases from seismic noise and signal coda, in identifying regional phases, and in separating the various phases of mixed events.

SECTION V
CONCLUSIONS AND RECOMMENDATIONS

A. CONCLUSIONS

The following conclusions are drawn from the work performed on the phase-difference polarization filter:

- Using batch processing, a broadband bandpass filter (in this study, 0.5-5.0 Hz) is more effective as a preprocessor to the polarization filter than is an arbitrary narrowband filter;
- Choice of the processing segment length used in the polarization filter algorithm appears to have a greater effect on the signal-to-noise ratio improvement of short-period regional phases than does the choice of the trapezoidal pass window half-width parameters for the range of values tested (half widths of 10^{o} to 20^{o});
- The 'best' results, in terms of signal-to-noise ratio gain, are obtained with a polarization filter processing segment length of 16 points;
- The polarization filter provides signal-to-noise ratio gains of approximately 10 dB for regional compressional and shear waves, and of approximately 8 dB for Lg and Rg;
- Direct estimates of detection capability improvement which result from application of the phase-

difference polarization filter for regional P and S waves were found to be approximately 0.6 m_b units;

- In addition to its use as a signal extractor, the phase-difference polarization filter can be used to separate mixed signals and to identify phases.

B. RECOMMENDATIONS FOR FUTURE USE

The following recommendations should be considered in any future work involving the phase-difference polarization filter:

- Implement the phase-difference polarization filter in an interactive processing environment;
- Cascade the phase-difference polarization filter with the previously-developed particle-motion polarization filter (Strauss, 1978) which tests on the angle of incidence to create a total model of bodywave polarization;
- Test the phase-difference polarization filter on data recorded at a different station in order to check for regional dependence of program parameters and in order to estimate better the Lg and Rg extraction results.

NOTE:

Advanced applications of polarization filtering should address a more complete interpretation of phase arrival times and of the relation of these arrivals to local crustal structure. Also, the relative excitation and frequency of phases

can be used to determine information on source depth and source mechanism. This important application can be facilitated by further development of interactive waveform extraction combined with synthetic studies which would be used to predict the observed wavetrain associated with specific source region-to-station paths. Results shown here, with a few of the better known phases, indicate interesting possibilities for applying this approach to precise seismic interpretation of observed phases.

Criteria for, and the precision of, source direction and distance determinations should be thoroughly evaluated. The combined use of the phase associations with source distance, direction, and depth estimates may provide the only feasible basis for focal determinations and discrimination of small regional events.

SECTION VI
REFERENCES

Brand, L., 1955; Advanced Calculus, John Wiley and Sons, Inc., New York, NY.

Ewing, W. M., W. S. Jardetzky, and F. Press, 1957; Elastic Waves in Layered Media, Lamont Geological Observatory Contribution Number 189, McGraw-Hill Book Company, New York City, NY.

Herrin, E., and J. Richmond, 1960; On the Propagation of the Lg Phase, Bulletin of the Seismological Society of America, Volume 50, Number 2, 197-210.

Jeffreys, H., and K. E. Bullen, 1967; Seismological Tables, British Association for the Advancement of Science, London, Great Britain.

Lane, S. S., 1973; Evaluation of the Adaptive Three-Component Lamont Processor, Special Report No. 15, Texas Instruments Report No. ALEX(01)-STR-73-15, AFTAC Contract Number F33657-72-C-0725, Texas Instruments Incorporated, Dallas, TX.

Lane, S. S., 1976; Development of Three Signal Processing Techniques, Technical Report No. 6, Texas Instruments Report No. ALEX(01)-TR-76-06, AFTAC Contract Number F08606-76-C-0011, Texas Instruments Incorporated, Dallas, TX.

Lane, S. S., 1977; Extraction of Long-Period Surface Waves, Technical Report No. 8, Texas Instruments Report No.

ALEX(01)-TR-77-08, AFTAC Contract Number F08606-77-C-0004, Texas Instruments Incorporated, Dallas, TX.

Ringdal, F., 1974; Estimation of Seismic Detection Thresholds, Technical Report No. 2, Texas Instruments Report No. ALEX(01)-TR-74-02, AFTAC Contract Number F08606-74-C-0033, Texas Instruments Incorporated, Dallas, TX.

Strauss, A. C., 1976; Evaluation of the Improved Three-Component Adaptive Processor, Technical Report No. 7, Texas Instruments Report No. ALEX(01)-TR-76-07, AFTAC Contract Number F08606-76-C-0011, Texas Instruments Incorporated, Dallas, TX.

Strauss, A. C., 1978; Extraction of Seismic Waveforms, Technical Report No. 14, Texas Instruments Report No. ALEX(01)-TR-78-02, AFTAC Contract Number F08606-77-C-0004, Texas Instruments Incorporated, Dallas, TX.

Unger, R., 1978; Automatic Detection, Timing and Preliminary Discrimination of Seismic Signals with the Instantaneous Amplitude, Phase and Frequency, Technical Report No. 4, Texas Instruments Report No. ALEX(01)-TR-77-04, AFTAC Contract Number F08606-77-C-0004, Texas Instruments Incorporated, Dallas, TX.

APPENDIX A
THE POLARIZATION FILTER PROGRAM

This appendix describes the operation of the polarization filter program as it is presently constituted.

Figure A-1, a flow diagram of the polarization filter program, shows the steps taken in processing data. Data to be processed consist of a maximum of 409.6 seconds of short-period data (4096 data points sampled at 10 points per second), the horizontal components of which have been rotated from their recorded north-south, east-west orientation to a transverse, radial orientation.

Once entered into the program, the data are first bandpass filtered to provide a standard against which to compare the polarization filter output. Next, the RMS noise, peak signal amplitudes, and signal-to-noise ratios for the compressional, shear, and surface waves are computed from the bandpass filtered data. The bandpass filtered data next serve as input to the polarization filter algorithm in order to achieve maximum SNR gain (this filter cascading approach was developed by Lane (1977) and Strauss (1978)).

The next step in the processing sequence is to check a set of flags input to the program to determine the type of waveform (compressional, retrograde elliptical, shear, or prograde elliptical) the polarization filter algorithm is to pass. Each of the four flags either has a value of zero

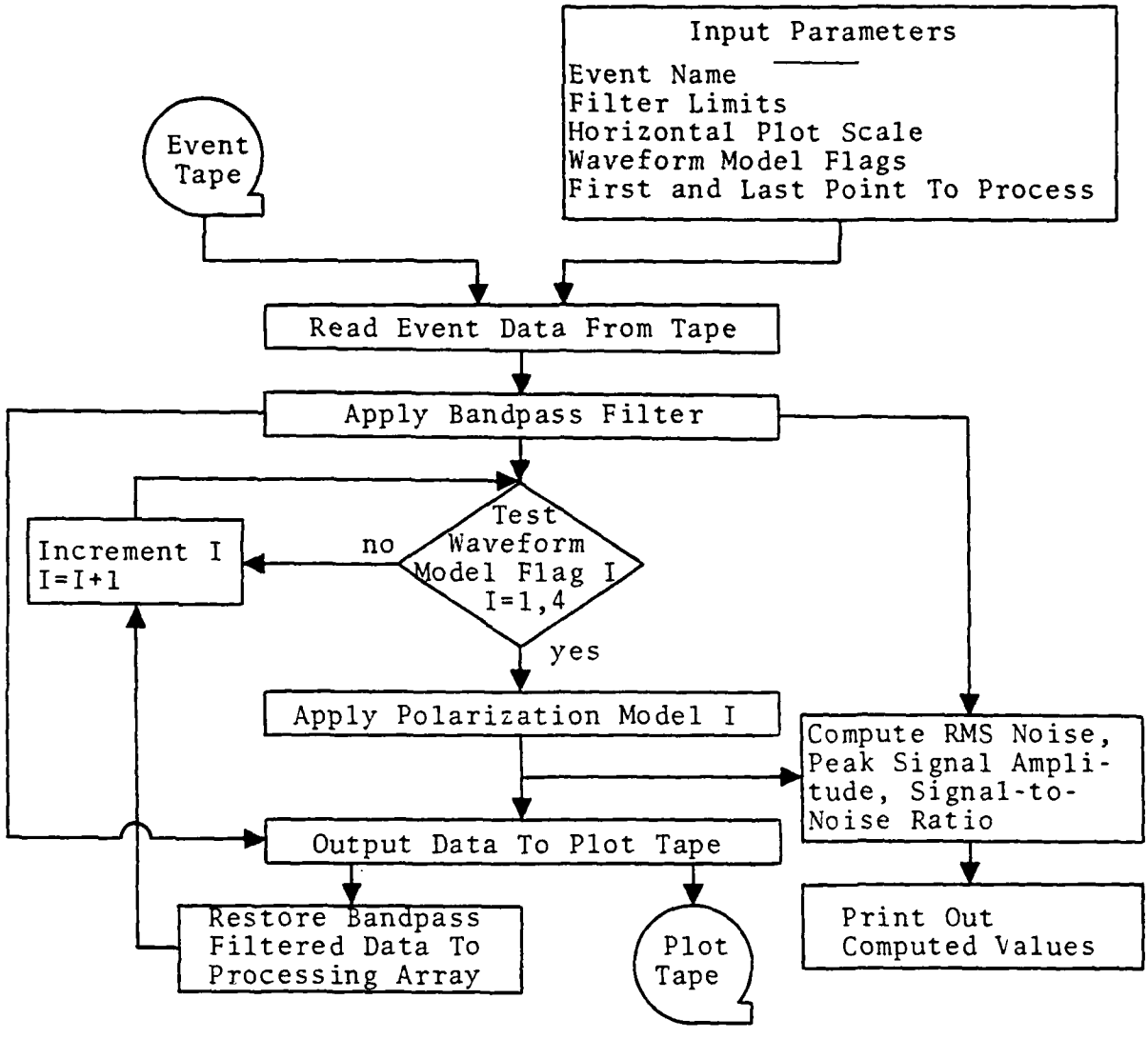

FIGURE A-1

GENERALIZED FLOW OF PHASE-DIFFERENCE POLARIZATION FILTER

denoting no polarization filtering is to be performed for this model, or one denoting polarization filtering is to be performed. Thus, if the first flag is set to one, the compressional waveform model of the polarization filter is applied. Upon completion of waveform processing, the second flag is tested to determine whether the retrograde elliptical waveform model is to be applied. Following this, the third flag is tested to determine whether the shear waveform model is to be applied, and, finally, the fourth flag is tested to determine whether the prograde elliptical waveform is to be applied.

Once the program has determined that a particular model is to be applied, the controlling parameters of the polarization filter algorithm (i.e., the number of points per processing segment, and the width of the pass window) are set to their pre-determined values. The bandpass filtered data are then polarization filtered according to the selected model. From the filtered data, the RMS noise, peak signal amplitude, and SNR are computed, and the filtered data are written on a plot tape. The program then restores the bandpass filtered data and loops back for the next waveform model. The RMS noise, peak signal amplitude, and signal-to-noise ratio computed before and after polarization filtering are printed out to allow computation of noise suppression, signal degradation, and signal-to-noise ratio improvement due to the polarization filter.

Figure A-2 is a detailed flow diagram of the polarization filter algorithm. To begin, the first data segments (say, 32 points of the vertical, radial, and transverse traces) are moved into a processing array. Next, the mean

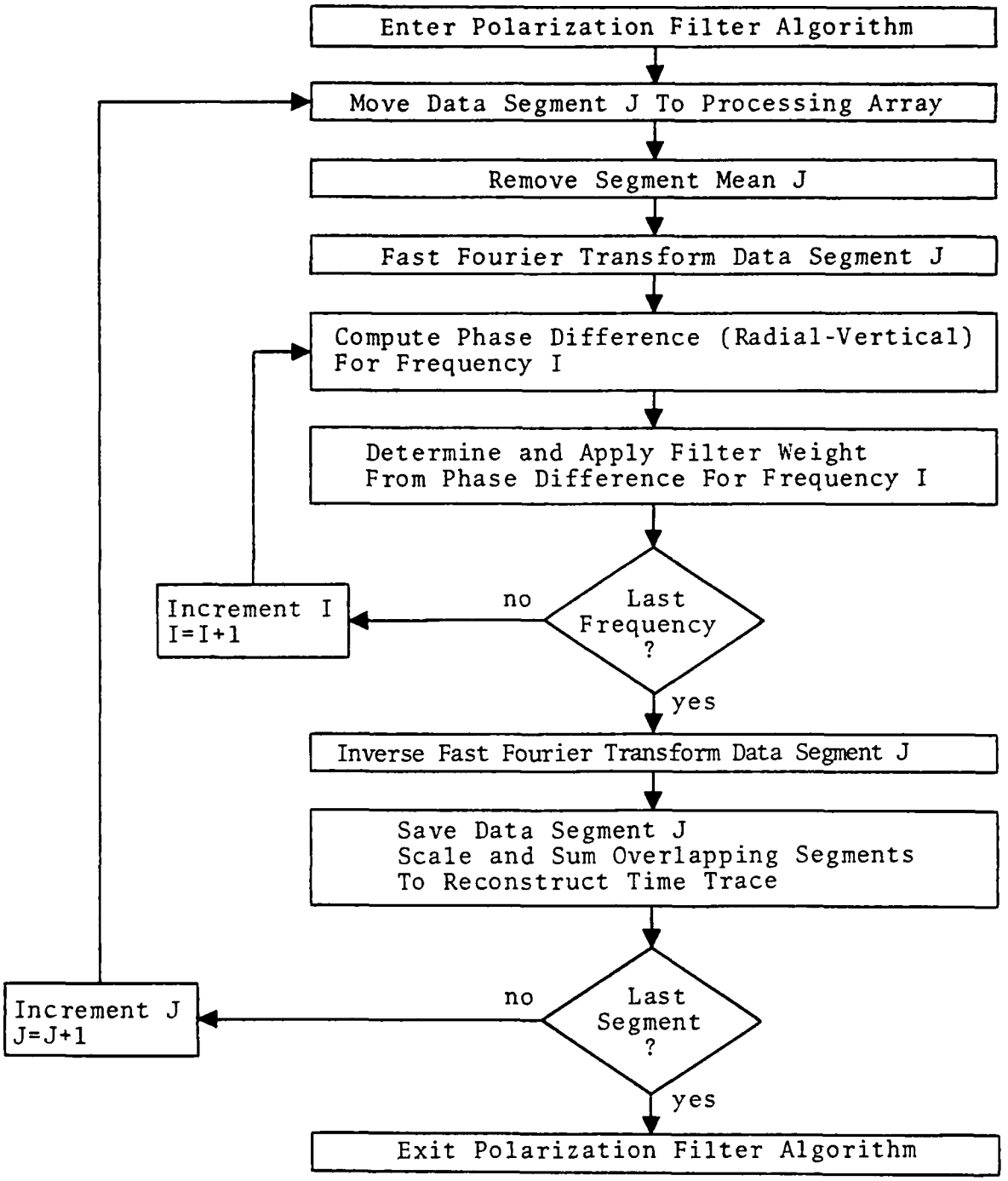

FIGURE A-2

DETAILED FLOW OF POLARIZATION FILTER ALGORITHM

of each data segment is removed, the processing array is padded with zeros to eight times the segment length, and the resulting zero-mean data are Fourier transformed. The algorithm then enters a loop on the number of discrete frequencies. For each frequency, the difference in phase between the radial and vertical components is computed. This phase difference is then compared to the trapezoidal pass window (shown in Figure A-3), which is centered on the expected phase difference for the waveform model under consideration. The filter weight for this frequency, as determined by this comparison, is then applied to the data at that frequency. Specifically, it is applied to three traces for the compressional and shear models, and to the vertical and radial components for the retrograde and prograde elliptical models.

The purpose in applying the filter weights to the transverse component in the compressional case is to pass any compressional energy present. Significant amounts of compressional energy on this component indicate an off-azimuth arrival; i.e., the waveform being extracted is not from the expected source. Applying the filter weights to the transverse component in the shear case permits extraction of S_H, which arrives at the same time as S_V. For the retrograde and prograde elliptical models, the transverse data segment is processed by a separate algorithm which is designed to extract Love waves. This algorithm tracks the incoming Love wave in azimuth and rejects all energy with approach azimuths outside a preset range centered on the great circle azimuth (see Strauss, 1976).

After completion of the loop on frequencies, the polarization-filtered segments are inverse fast Fourier

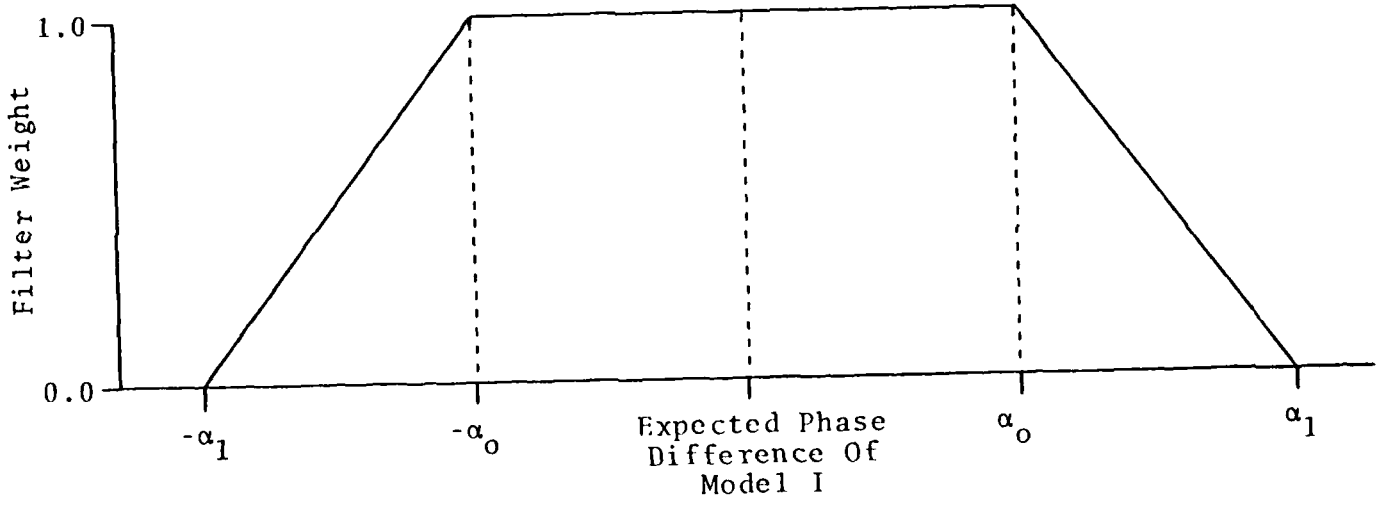

FIGURE A-3

POLARIZATION FILTER TRAPEZOIDAL PASS WINDOW
(α_o, α_1 are preset filter parameters)

transformed and saved. Ensuing segments each overlap the preceding segment by 50 percent. After processing, the overlapping data points are scaled and summed to construct the polarization-filtered time traces.